Arabian Journal of Chemistry (2022) **15**, 103925

King Saud University

Arabian Journal of Chemistry

www.ksu.edu.sa
www.sciencedirect.com

ORIGINAL ARTICLE

Insight into the performance of novel kaolinite-cellulose/cobalt oxide nanocomposite as green adsorbent for liquid phase abatement of heavy metal ions: Modelling and mechanism

Daud Hussain [a], **Suhail Ayoub Khan** [a], **Salman S. Alharthi** [b], **Tabrez Alam Khan** [a,*]

[a] *Department of Chemistry, Jamia Millia Islamia, Jamia Nagar, New Delhi 110 025, India*
[b] *Department of Chemistry, College of Science, Taif University, P.O. Box 110999, Taif 21944, Saudi Arabia*

Received 11 March 2022; accepted 12 April 2022
Available online 20 April 2022

KEYWORDS

Kaolinite;
Cellulose;
Green Co_3O_4;
Nanocomposite;
Adsorption;
Isotherm

Abstract A cost-efficient kaolinite-cellulose/cobalt oxide green nanocomposite (Kao-Cel/Co_3O_4 NC) was successfully synthesized, and utilized as a promising material for removing Pb^{2+} and Cd^{2+} from aqueous solution. The fabricated nanocomposite has been characterized by Fourier transform infrared spectroscopy, X-ray diffraction, scanning electron microscopy-energy dispersive X-ray, high-resolution transmission electron microscopy, and Brunauer-Emmett-Teller analysis. The batch methodology was exploited for optimization of process parameters and the optimized conditions were found to be adsorbent dosage (2.0 g/L), extraction time (50 min), initial concentration (60 mg/L), and initial solution pH (6). Kao-Cel/Co_3O_4 NC displayed excellent adsorption properties and achieved maximum saturation capacity (Q_m) of 293.68 mg Pb^{2+}/g and 267.85 mg Cd^{2+}/g, with an equilibration time of 50 min at 323 K. The Langmuir model best expressed the isotherm data recommending the adsorption onto energetically homogeneous NC surface, while the compatibility of kinetics data with pseudo-second-order model revealed the dependency of adsorption rate on adsorption capacity, and probable involvement of chemisorption in the rate-controlling step. Electrostatic interaction and ion exchange mechanism were responsible for the uptake of Pb^{2+} and Cd^{2+} by Kao-Cel/Co_3O_4 NC as demonstrated by Fourier transform infrared spectroscopy and pH studies. Thermodynamic parameters confirmed the physical, spontaneous, and endothermic sequestration processes. Real water investigation specified that the present adsorbent could be effectively used for liquid phase decontamination of Pb^{2+} and Cd^{2+}. The nanocomposite exhibited high reusability, which could be utilized efficiently for five runs with sustainable

* Corresponding author.
E-mail address: takhan@jmi.ac.in (T.A. Khan).
Peer review under responsibility of King Saud University.

Production and hosting by Elsevier

https://doi.org/10.1016/j.arabjc.2022.103925

results. In summary, this study portrayed the present nanocomposite as an emerging material for the adsorption of heavy metal ions particularly Pb^{2+} and Cd^{2+}.

1. Introduction

The upsurge in heavy metals (with specific gravity > 5 g/cm^3) level caused due to the release of metals-rich effluents from industries such as fertilizers, chemicals, metallurgical, leather, metal finishing, and plating into aquatic resources significantly impacts the health of the ecosystem owing to their potential toxicity and bioaccumulating propensity in the living organisms. Although most heavy metals are believed to be biologically insignificant, the trace amounts of a few of them like Fe^{2+}, Co^{2+}, Cu^{2+}, Zn^{2+}, and Mn^{2+} play beneficial roles in mammalian metabolic systems. The presence of intensified quantities of heavy metals in the ecosystem constitutes severe environmental challenges causing a hazardous impact on humans and biotic life (Saravaia et al., 2018). Metals are most pernicious in the ionic forms (Ni^{2+}, Cd^{2+}, Pb^{2+}, Hg^{2+}, Cr^{6+}, $As^{3+(5+)}$) that can react with biomolecules forming stable toxicants, which are difficult to dissociate. However, exposure to Pb^{2+} and Cd^{2+} are toxic even at trace concentrations that can cause serious damage to human and animals health due to their bioaccumulation in the body (Mnasri-Ghnimi and Frini-Srasra, 2019). Overexposure to Cd^{2+} can perpetrate acute respiratory distress syndrome and lung disorders causing emphysema, pulmonary edema and dyspnea, tachycardia, anemia, cyanosis of skin and mucous membranes, anosmia, tubular necrosis of the kidney, osteomalacia, and improper liver functioning. Besides, it may also produce nausea, vomiting, diarrhea, abdominal cramps, headaches, and fatigue. Since Pb^{2+} is exceedingly environmentally persistent, its acute exposure poses a distressing impact on the hematopoietic, renal, reproductive, and central nervous systems, caused chiefly due to enhanced oxidative stress (Flora et al., 2012). The major symptoms of Pb^{2+} poisoning include hypertension, fatigue, lethargy, anorexia, insomnia, anemia, peripheral neuropathy, encephalopathy, ataxia, kidney disease, and behavioral changes (Wani and Usmani, 2015). Hence, to minimize the toxicological effects of Pb^{2+} and Cd^{2+} on human health and to preserve the aquatic environment, it is imperative to adsorb these undesirable metals from aqueous industrial wastes or contaminated water (Saravaia et al., 2018).

Various wastewater remediation approaches including ion exchange, ultrafiltration, chemical/electrochemical oxidation, coagulation/electrocoagulation, chemical precipitation, reverse osmosis, photocatalytic/microbial degradation, and adsorption have been probed for the decontamination of heavy metals from the aqueous system. But most of these techniques experience limitations due to intricate operations, unprofitability, disposal issues, and sometimes poor removal efficiency. But the adsorption process is extensively used for the elimination of wide-ranging pollutants from industrial wastewater (Javid and Malakootian, 2017; Khan and Khan, 2021; Malakootian et al., 2019). Adsorption is an economic-friendly, technically feasible, and efficient process for the purging of heavy metals from wastewater. Adsorption has many advantages over other methods, which include simple design, ease of operation at mild conditions and wide pH range, effectiveness at low contaminant concentrations, availability of variety of adsorbent materials, selectivity, and regenerability. However, the process is often afflicted with poor specificity, indecorous adsorbent disposal, and regular replacement of spent adsorbents. A variety of conventional low-cost adsorbents encompassing agricultural and industrial waste materials, nanomaterials, and nanocomposites have been efficaciously invoked for the separation of heavy metals from industrial effluents (Khan et al., 2016; Khan et al., 2009; Khan et al., 2016; Gu et al., 2019). During the last years, clays and their composites have been utilized as extremely efficient and economically-feasible adsorbents for the cleansing of metals-containing water owing mainly to their high microporosity, large specific surface area, high cation exchange capacity, surface hydrophilicity/electronegativity, good swelling ability, high stability and environmental safety (Yadav et al., 2019; Adebowale et al., 2006). Kaolinite, an aluminosilicate clay with a 1:1 dioctahedral layered structure having one SiO_4 tetrahedral sheet and one $Al(OH)_3$ octahedral sheets in each layer; held together by an O—H—O bond between the adjacent layers, can serve as adsorbing material for eradicating diverse contaminants from wastewater (España et al., 2019). However, raw kaolinite suffers from relatively low adsorption capacity, and lower CEC (3–15 mEq/100 g) as compared to montmorillonite/bentonite or activated carbon and the adsorption uptake of pollutants by natural minerals might diminish after a few cycles. However, several modification methods of clays such as thermal or acid/base activation, pillarization, metal oxide coatings, or intercalation have led to good adsorbents with improved sorption efficiency because of increased pore size and volume, specific surface area, and surface binding sites (Khan et al., 2015, 2017). In recent times, biopolymer/clays bionanocomposites have garnered considerable attention as captivating materials for the attenuation of contaminants from polluted water on account of their boosted biodegradability and biocompatibility due to biopolymers, the improved high surface area, increased number of adsorption sites, and the admirable sorption capacity of clays (Del Mar Orta et al., 2020). Among numerous biopolymers such as starch, alginate, or chitosan, cellulose, a ubiquitous and renewable biopolymer with plentiful natural availability, is of considerable interest because of its biocompatibility, biodegradability, high mechanical strength, eco-efficacy, non-hazardous, and excellent adsorption capacity resulting from the presence of plenty of —OH groups. In this context, cellulose-based materials (Jamshaid et al., 2017), hydrogels (Akter et al., 2021) and composites (Ajala et al., 2022) have been usually applied for the uptake of numerous pollutants including heavy metals from wastewater. Many cellulose/clays composites such as cellulose-montmorillonite for Cr^{6+} (Kumar et al., 2012), and montmorillonite cellulose nanocomposite for Cu^{2+} and Cd^{2+} (Abunah et al., 2019) removal have been reported. Recently, cellulose/bentonite-zeolite composite

(Shamsudin et al., 2019), and cellulose@organically modified montmorillonite (Cai et al., 2017) have been studied for the removal of brilliant green and Cr^{6+}; respectively from water.

In this work, cellulose, a long-chain natural polymer with repeating units of β-D-glucose, was suitably utilized for green functionalization of kaolinite through intercalation, and its subsequent compositing with green-synthesized Co_3O_4 NPs for application as a novel adsorbent for removal of heavy metals (Pb^{2+}, Cd^{2+}) from an aqueous phase. Kaolinite, low-cost natural material was implemented for the synthesis of the nanocomposite due to its extensive availability, flexible chemical and crystalline structure, high ion exchangeability, innocuous nature, and promising adsorption capabilities. In the recent past, the green synthesis, an eco-compatible, nontoxic, and economical methodology has caught much attention to obtain nanomaterials utilizing extracted phytochemicals from the plant parts, which display reducing effects (Jadoun et al., 2021; Khan et al., 2018) and further serve as capping agents that minimize the agglomeration of the target nanoparticles (Vidovix et al., 2019). The present study aims to produce a novel green adsorbent, kaolinite-cellulose/Co_3O_4 nanocomposite using green fabricated cobalt oxide nanoparticles (Co_3O_4 NPs) with improved adsorption capacity for Pb^{2+} and Cd^{2+} decontamination from aqueous solution. The effect of different parameters including initial metal concentration, adsorbent mass, agitation time, and operating solution pH on adsorption efficiency was also studied. The effectiveness of adsorption properties and performance was appraised through modelling of relevant data using different adsorption isotherm and kinetic models; and thermodynamic parameters. The reusability and performance evaluation in real wastewater of the present adsorbent was also explored.

2. Experimental

2.1. Material, methods, and instruments

Kaolinite (Shree Ram Minerals, Gujarat), cellulose acetate (Merck, India), lead nitrate, cadmium nitrate, cobalt nitrate (Merck, India), ethanol, dithizone, cetyltrimethylammonium bromide (CTAB), ammonium persulfate (APS) (all Merck, India), and HCl (Fischer Scientific, India) of analytical grade were used as acquired. The characterization of Kao-Cel/Co_3O_4 NC was accomplished using Fourier transform infrared spectroscopy, (FTIR) {Perkin-Elmer spectrometer, model BX spectrum, USA}, X-ray diffraction (XRD) {Philips Analytica PW 1830 apparatus, Philips, Netherlands}, Brunauer–Emmet t–Teller (BET) {BET surface area analyzer (Quantachrome NovaWin}, Scanning electron microscope (SEM) {Carl Zeiss JOEL scanning electron microscope, Sigma 5.05, Germany}, energy dispersive X-Ray analysis (EDX) {Team EDS system, EDAX Inc.}, transmission electron microscopy (TEM) (Transmission electron microscope, HRTEM 200 kV model, FEI Tecnai), and the solution pHs was measured utilizing the Decibel pH meter (model DB-1011).

2.2. Synthesis of the cellulose functionalized kaolinite (kaolinite-cellulose)

The preparation of the modified kaolinite using cellulose as an intercalating biopolymer may be summarized as follows: Kaolinite (5 g) was dispersed in 100 mL of deionized water by stirring for 1 h, and then 0.1 g of CTAB solution was added and stirring further continued for 12 h. To this mixture, an ethanolic dispersion (50 mL) of cellulose (2.5 g) was mixed under continuous stirring for another 2 h. Thereafter, the kaolinite-cellulose mixture was exposed to ultrasonic irradiation for 5 h to accelerate the intercalation of cellulose between the kaolinite interlayers.

2.3. Green fabrication of kaolinite-cellulose/cobalt oxide nanocomposite

Plant leaf extract of *Berberis lycium* in ethanol was used as a capping and reducing agent for the precipitation of cobalt oxide over the kaolinite-cellulose clay (Kao-Cel). Firstly, 3.0 g of the pre-prepared Kao-Cel was suspended in 100 mL double-distilled water and sonicated for 1 h. Afterward, cobalt nitrate solution (2.5 g in 100 mL distilled water) was mixed with Kao-Cel suspension under constant stirring at 500 rpm. Then, 50 mL of *Berberis lycium* extract was added into the solution mixture under constant stirring and left for 48 h to affect the complete precipitation of nano cobalt oxide over Kao-Cel. The obtained residue of kaolinite-cellulose/cobalt oxide nanocomposite, abbreviated as Kao-Cel/Co_3O_4 NC, was separated by centrifugation, washed with deionized water, dried in an oven at 80 °C for 12 h, and finally preserved in a desiccator.

2.4. Equilibrium adsorption studies

In the present study, the adsorptive capacity or the removal effectiveness of the Kao-Cel/Co_3O_4 NC towards the target pollutants was evaluated by conducting a number of equilibrium adsorption experiments by agitating a constant adsorbent mass with a series of solutions of different [Pb^{2+}] or [Cd^{2+}] prepared from a stock solution of 500 mg/L each. The batch mode techniques were employed to study the impact of different process variables such as agitation time, adsorbent mass, initial metal concentration, pH, and temperature on adsorption. To an aliquot of 25 mL of metals solution (20–80 mg/L) in an Erlenmeyer flask (50 mL) was added a fixed adsorbent mass (0.4–2.4 g/L), and the solution mixture was shaken on a water bath shaker at a different time of agitation (10–60 min), pH (2.0–10) and temperature (303 K, 313 K and 323 K). After equilibrium was attained, the sorbent was separated by centrifugation and the centrifugate was investigated using T80 + UV/Vis spectrophotometer, PG Instrument Ltd, UK. The UV/Vis analyses of the test solutions for determining Pb^{2+}/Cd^{2+} concentration was performed according to standard procedure using dithizone as a complexing agent (Khan et al., 2016; Khan et al., 2007). Briefly, 2.0 mL of dithizone solution and 1.0 mL of HCl (0.1 M) was mixed with Pb^{2+}/Cd^{2+} solution, followed by 2.0 mL of CTAB solution (0.3 M). The absorbance of the colored solutions thus developed was measured along with the corresponding blank at λ_{max} of 505 nm (Pb^{2+}) and 540 nm (Cd^{2+}). The remanent concentrations of Pb^{2+}/Cd^{2+} post-adsorption was determined from the linear calibration curve obtained by plotting the absorbance versus Pb^{2+}/Cd^{2+} concentration (5–30 mg/L) (Fig. S1) with $R^2 = 0.994$ showing good correlation. The limit of detection for Pb^{2+} and Cd^{2+} was appraised from the

straight-line calibration plot, which was found to be 0.464 and 0.591 μg/L, respectively. For isotherm experiments at 303, 313, and 323 K, a 2.0 g/L Kao-Cel/Co_3O_4 NC was shaken with different initial Pb^{2+} or Cd^{2+} concentrations (20–80 mg/L) for 50 min extraction time at pH 6. However, the kinetic measurements were accomplished at constant temperature (303 K) by agitating 25 mL of Pb^{2+} or Cd^{2+} (40, 50, and 60 mg/L) by applying a fixed sorbent mass (2.0 g/L) for 10–60 min (10 min interval) and pH 6.

The adsorptive capability of Pb^{2+} and Cd^{2+} (q_t, mg/g) onto the sorbent surface at a given time (min) and removal efficiency (R) was deduced from the equilibrium adsorption data based on the mass balance relationship (Eq. (1)) and Eq. (2), respectively:

$$q_t\left(\frac{\text{mg}}{\text{g}}\right) = \frac{(C_i - C_t)V}{w} \tag{1}$$

$$R(\%) = \frac{(C_i - C_e)}{C_i} \times 100 \tag{2}$$

where, C_i, C_t, and C_e (mg/L) are the initial Pb^{2+} or Cd^{2+} concentration, at the time, t, and at equilibrium, respectively, V (L) is the volume of the aqueous system and w (g) is the mass of the sorbent.

The fitting of the equilibrium data to various isotherm model equations affords many physically meaningful constants, which may provide insight into the surface properties, sequestration capacity, heterogeneity of the adsorbent, mechanism of adsorption, affinity towards adsorbate, and energy of adsorption. The data was evaluated using Langmuir (Langmuir, 1918); Freundlich (Freundlich, 1906); Temkin (Temkin, 1940), and Dubinin–Radushkevich (D–R) (Dubinin and Radushkevich, 1947) isotherm model equations at 303 K, 313 K, and 323 K by applying nonlinear regression analysis. The corresponding nonlinear isotherm equation is listed in Table 1. The study of adsorption kinetics is essential to acquire information regarding the pollutants uptake rate, which controls the contaminant's residence period at the sorbent-sorbate interface, and interpret the plausible adsorption mechanism. The kinetic data is analyzed by applying Lagergren pseudo-first-order (Lagergren, 1898), Ho's pseudo-second-order (Ho and McKay, 2003), Weber-Morris intra-particle diffusion (Weber and Morris, 1963), and Boyd liquid film diffusion (Boyd et al., 1947) model equations (Table 3) to determine the rate of Pb^{2+} or Cd^{2+} adsorption and the underlying mechanism thereof. Thermodynamic parameters such as a change in entropy (ΔS^o), enthalpy (ΔH^o), and Gibbs free energy (ΔG^o) were determined by van't Hoff equation ($\ln k_c = -\frac{\Delta H^0}{RT} + \frac{\Delta S^0}{R}$) and Gibbs equation ($\Delta G^\circ = \Delta H^\circ - T\Delta S^\circ$) to evaluate the change in randomness at the sorbate-sorbent interface, endothermic/exothermic nature, feasibility and spontaneity of the sorption procedure, respectively.

In desorption studies, 2.0 g/L of Kao-Cel/Co_3O_4 NC was saturated with Pb^{2+} or Cd^{2+} solution (50 mg/L) for 1 h. The used adsorbent was regenerated by agitating it with HCl (0.1 M), NaOH (0.1 M), or ethanol for 10 min, washed, dried in an oven, and reused. The Kao-Cel/Co_3O_4 NC shows good regeneration ability towards NaOH. To check the recyclability of the present adsorbent, the adsorption-desorption experiments were performed up to five cycles, and the confiscation capacity of the adsorbent was assessed. Similarly, in order to appraise the competence of Kao-Cel/Co_3O_4 NC to adsorb Pb^{2+} and Cd^{2+} from real wastewater, water sample from the light vehicles washing area of a local garage (pH = 7.6; COD = 207 mg/L; Total solids = 1275 mg/L; Total suspended solids = 700 mg/L; Oil and grease = 50 mg/L) was collected, allowed to stand for 24 h. The supernatant (5.0 mL) was diluted to 100 mL, and spiked with Pb^{2+} or Cd^{2+} solutions (30–80 mg/L).

3. Results and discussion

3.1. Characterization of Kao-Cel/Co_3O_4 nanocomposite

3.1.1. Fourier transform infrared (FTIR) spectra

The FTIR spectra of kaolinite (Kao), cellulose (Cel), kaolinite-cellulose clay (Kao-Cel), and Kao-Cel/Co_3O_4 NC are shown in Fig. 1. The absorption bands appearing at 3670 cm^{-1} and

Table 1 Isotherm model parameters, R^2 and error function values.

Model/Equation	Parameters	Pb^{2+}			Cd^{2+}		
		303 K	313 K	323 K	303 K	313 K	323 K
Langmuir	Q_m	155.78	249.84	293.68	132.35	215.95	267.85
$q_e = \frac{Q_m b_L C_e}{1+b_L C_e}$	b_L	0.091	0.077	0.044	0.682	0.402	0.367
	R^2	0.989	0.992	0.998	0.985	0.991	0.996
	SEE	0.340	0.280	0.260	0.682	0.484	0.296
Freundlich	K_F	17.48	19.27	20.52	17.01	17.22	18.67
$q_e = K_F C_e^{\frac{1}{nF}}$	$1/n_F$	0.813	0.830	0.885	0.523	0.526	0.511
	R^2	0.964	0.983	0.991	0.950	0.958	0.967
	SEE	3.113	2.136	0.680	2.779	2.776	1.576
Temkin	K_T	1.35	1.34	1.31	3.69	3.60	3.99
$q_e = \beta_T \ln(K_T C_e)$	b_T	0.074	0.073	0.071	0.199	0.197	0.183
	R^2	0.971	0.988	0.996	0.965	0.978	0.985
	SEE	2.790	1.733	1.047	2.530	2.247	1.833
D–R	$q_{D\text{-}R}$	117.09	120.69	121.83	117.24	119.77	120.81
$q_e = q_{D-R}\exp\left[-K_D\left(1+\frac{1}{Ce}\right)^2\right]$	$E_{D\text{-}R}$	0.348	0.337	0.314	0.351	0.339	0.319
	R^2	0.982	0.987	0.992	0.961	0.966	0.976
	SEE	2.161	1.861	1.419	3.003	2.786	2.352

Table 2 Comparison of Q_m (mg/g) values with other adsorbents.

Adsorbent	Experimental conditions				Q_m (Pb^{2+}) (mg/g)	Q_m (Cd^{2+}) (mg/g)	Kinetics/ Isotherm	Ref.
	Conc (mg/L)	pH	Dose (g/L)	Temp (K)				
Sulfhydryl functionalized hydrogel	100	5–6	0.2	298	38.69	27.37	Pseudo-second order/ Langmuir	(Hua and Li, 2014)
Amino-functionalized magnetite/ kaolin clay	100 Pb^{2+} 30 Cd^{2+}	2.5 8.3	0.08 0.05	298	86.1	22.1	Pseudo-second order/ Langmuir	(Qin et al., 2016)
Iron oxide modified clay composite beads	50	4	2	298	74.20	41.30	Pseudo-second order/ Langmuir	(Pawar et al., 2018)
Modified gum tragacanth/graphene oxide composite	60	6	0.02	298	142.50	112.50	Pseudo-second order/ Langmuir	(Sahraei and Ghaemy, 2017)
Gelatin bentonite composite	58.37	5	0.1	298	47.16	–	Pseudo-second order/ Langmuir	(Pal et al., 2017)
DMSA@Fe_3O_4 MNRs	20	5	0.1	301	46.18	–	Pseudo-second order/ Langmuir/ Freundlich	(Venkateswarlu et al., 2019)
EDTA-SWCNTs	10	5	0.1	313	204.1	188.7	Langmuir	(Fard et al., 2022)
Sustainable biochar from saw dust	180	5	0.1	298	58.85	44.20	Pseudo-second order/ Langmuir	(Cheng et al., 2021)
Oxidized D. *dumentorum* starch-NPs	50	–	0.05	323	88.49	96.15	Pseudo-second order/ Freundlich	(Awokoya et al., 2021)
SH–SiO_2MS-Ca-Al	10	6	0.3	333	127.99	70.68	Pseudo-second order/ Langmuir	(Singh et al., 2022)
Oak wood ash/GO/Fe_3O_4	10	6	1	298	47.16	43.66	Pseudo-second order/ Langmuir	(Pelalak et al., 2021)
Corn straw biochar	20	4.5	1	–	28.99	38.91	Langmuir	(Chi et al., 2017)
PAAm/bentonite hydrogel nanocomposite	30	6	2	323	138.33	200.41	Pseudo-second order/ Freundlich	(Khan et al., 2021)
Kao-Cel/Co_3O_4 nanocomposite	50	6	2	323	293.67	267.84	Pseudo-second order/ Langmuir	Present study

1640 cm^{-1} denote Al—OH stretching vibration of kaolinite, and H—O—H bond of water retained by the silica matrix (Fig. 1a) (Sari and Tuzen, 2014). The spectral band at 1122 cm^{-1} is assigned to Si—O stretching vibration (out of plane), while those at 1057 cm^{-1} and 948 cm^{-1} are attributed respectively to the stretching vibration of Si—O and —OH deformations of the inner surface hydroxyl groups. The bands corresponding to Si—O (deformation) and Al—O—Si (defor-

Table 3 Adsorption kinetics and diffusion parameters.

	Conc (mg/L)	Pseudo-firstorder $q_t = q_e(1 - e^{-k_1.t})$					Pseudo-second order $q_t = \frac{k_2 q_e^2.t}{(1+k_2 q_e.t)}$			
		k_1 (1/min)	R^2	*SEE*	q_e(exp) (mg/g)	q_e(cal) (mg/g)	k_2 (g/mg/min)	q_e(cal) (mg/g)	R^2	*SEE*
Pb^{2+}	40	0.453	0.829	0.077	23.66	23.62	0.255	23.74	0.975	0.018
	50	0.470	0.836	0.085	31.96	31.92	0.250	31.97	0.977	0.030
	60	0.505	0.816	0.082	40.34	40.29	0.241	40.41	0.978	0.033
Cd^{2+}	40	0.393	0.825	0.144	24.15	24.07	0.136	24.28	0.971	0.061
	50	0.419	0.822	0.152	32.52	34.44	0.131	32.66	0.926	0.072
	60	0.432	0.789	0.188	40.92	40.80	0.115	41.06	0.919	0.082
		Intra-particle diffusion $q_t = k_i.t^{0.5} + C_i$				Liquid-film diffusion $-\ln\left(1 - \frac{q_t}{q_e}\right) = k_A.t$				
		ki (mg/gmin$^{0.5}$)	*Ci*	R^2	*SEE*	k_A (1/min)	R^2	*SEE*		
Pb^{2+}	40	0.077	31.43	0.851	0.014	0.071	0.903	0.011		
	50	0.073	39.83	0.945	0.007	0.055	0.979	0.003		
Cd^{2+}	40	0.131	31.60	0.837	0. 025	0.099	0.912	0.017		
	50	0.156	39.83	0.919	0.020	0.086	0. 992	0.004		

mation) of the kaolinite is noticed at 748 cm^{-1} and 540 cm^{-1}, respectively (Khan et al., 2021). The Si—O—Si stretching peak is observed at 481 cm^{-1} (Khan et al., 2017). The characteristic absorption bands of cellulose (Fig. 1b) appear at 3465 cm^{-1} corresponding to O—H stretching vibration (Liu et al., 2017), and at 1368 cm^{-1}, 1225 $cm^{-1,}$ and 1036 cm^{-1} assigned respectively to C—CH_3 symmetric bending, asymmetric stretching of O—C═O group, and to asymmetric C—O—C stretching arising from the pyranose ring. Moreover, the band at 1738 cm^{-1} emerges due to the C═O of the acetate group in the cellulose (Ali et al., 2014; Yan et al., 2014; Khatri et al., 2012). The FTIR spectrum of Kao-Cel (Fig. 1c) validates the formation of hybrid material containing complex bands related to the functional groups of both kaolinite and cellulose, with observable deviations of characteristic groups from main positions. The fabrication of green Kao-Cel/Co_3O_4 nanocomposite is validated by the IR peaks in the spectrum of the composite material. Two new absorption peaks are observed for the Co_3O_4 structure as depicted in Fig. 1d. The peak at 541 cm^{-1} is attributed to Co—O stretching vibration and the band at 658 cm^{-1} is ascribed to O-Co-O bridging vibration (Manigandana et al., 2013; Farhadi et al., 2016). To scrutinize the functional groups that interact with Cd^{2+} and Pb^{2+} ions, the FTIR spectra of loaded-Kao-Cel/Co_3O_4 NC are revealed in Fig. 2a and b. Change in the position of some bands at 1734 and 1370 cm^{-1} and diminished intensities of bands at 1124, 1040, and 952 cm^{-1} support the successful uptake of Cd^{2+} and Pb^{2+} by the nanocomposite. The shifting or weakening of absorption bands corresponding to the O—H band and C═O/C—O stretching vibration indicates that free electron pairs on oxygen atoms in the hydroxyl and/or carboxyl groups interact with the empty orbitals of Pb^{2+} and Cd^{2+} to form complexes mediated by coordinative bonds, that alters the density of electron cloud causing the vibrational bands to shift or reduce in intensity (Wang et al., 2017; Haung et al., 2018; Jiang et al., 2019).

3.1.2. Brunauer–Emmett–Teller (BET) analysis

The specific surface area and porosity of the solid Kao-Cel/Co_3O_4 nanocomposite were determined from the nitrogen adsorption/desorption isotherm curves using the BET equa-

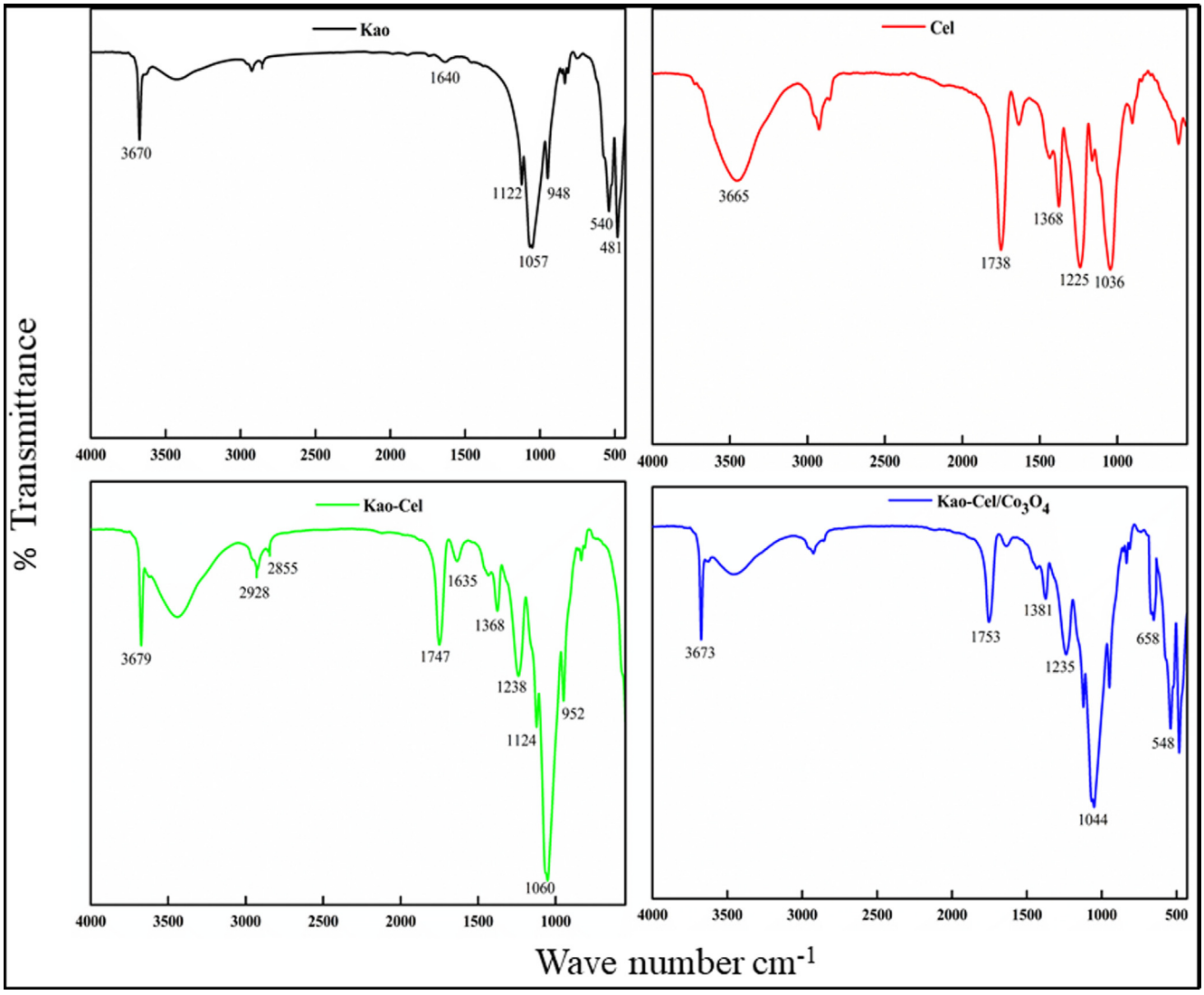

Fig. 1 FTIR spectra of Kao, Cel, Kao-Cel and Kao-Cel/Co_3O_4 nanocomposite.

tion. The N_2-adsorption/desorption isotherm and pore size distribution of Kao-Cel/Co_3O_4 NC are displayed in Fig. 3a and 3b, respectively, which reveals a small hysteresis loop that is categorized as type IV (Nguyen et al., 2017). The BET surface area of Kao-Cel/Co_3O_4 NC is 85.92 m^2/g, pore size determined by BJH is about 0.024 cm^3/g and a pore diameter is 7.221 nm, depicting the mesoporous nature of Kao-Cel/Co_3O_4 NC. The adsorbent surface area is an influential feature governing the adsorption of contaminants and thereby its effectiveness. Generally, a larger surface area means access to more active sites, and hence admirable adsorption aptitude.

3.1.3. X-ray diffraction (XRD) analysis

The structural features of Kao, Cel, Kao-Cel, and Kao-Cel/Co_3O_4 NC were approved by XRD as shown in Fig. 3c. The amorphous nature of cellulose, the crystallinity of kaolinite, and the nanocomposite are substantiated by the XRD patterns. The descriptive peaks are noticed at about 9.83° 19.30°, 26.77°, 29.32°, 35.34° 37.17°, and 49.37° for Kao. The intercalation of kaolinite sheets by cellulose is ascertained by the acquired XRD pattern of Kao/Cel, which displays that some reported peaks for Kao are shifted from the normal position with notable deviation in intensity. The principal peaks detected at 9.82° and 20.33° instead of 19.30° and 29.32° present in Kao, with a significant decrease in the intensities of these peaks, confirm the effective intercalation of Kao by Cel. In the obtained XRD pattern, the loading of Kao-Cel by cobalt oxide is discernable. The Kao-Cel/Co_3O_4 NC shows two additional peaks for cobalt oxide, which are observed at 30.96° and 45.55° (JCPDS No. 42-1467). The kaolinite (Kao) peaks appear much diminished in the NC which gives a strong indication that cobalt oxide precipitated onto the surface of the Kao/Cel. The average crystallite size of Kao-Cel/Co_3O_4 NC obtained using Scherrer formula is 43 nm.

3.1.4. Scanning electron microscopy-energy dispersive X-ray (SEM- EDX) analyses

The morphological features, shape, size, and elemental contents of the synthesized Kao-Cel/Co_3O_4 NC were scrutinized by SEM and EDX analysis. The SEM micrographs of Kao-Cel/ Co_3O_4 NC, before and after adsorption of Pb^{2+} and Cd^{2+}, are revealed in Fig. 4. The surface of the nanocomposite is figured out as irregular, rough, and highly porous due to the existence of sufficient pores and grooves of distinctive sizes and shapes, which are generally accountable for the larger surface area and higher adsorption efficacy of Kao-Cel/Co_3O_4 NC. However, the SEM images of Kao-Cel/Co_3O_4 NC post-sorption of Pb^{2+} and Cd^{2+} (Fig. 4b, 4c) display an almost smooth texture that validates the sorption of Pb^{2+} and Cd^{2+} onto Kao-Cel/Co_3O_4 NC surface. However, the EDX analysis recognizes the presence of additional elements, Pb or Cd in the Kao-Cel/Co_3O_4 NC adsorbent. after adsorption signifying the sorbed Pb^{2+} and Cd^{2+} onto the surface of the NC, and also validates the existence of Al, Si, O, C, and Co as the foremost components of the nanocomposite.

3.1.5. Transmission electron microscopy (TEM) analysis

The incorporation of green-synthesized cobalt oxide (Co_3O_4) nanoparticles, their size and shape, and size distribution were affirmed by TEM images, as depicted in Fig. 5a. The TEM images reveal the spherical Co_3O_4 nanoparticles randomly distributed within the kaolinite/cellulose (Kao-Cel) matrix, which may have resulted in significant augmentation in the textural properties and provide the nanocomposite with a high surface area. The particle distribution curve signifies that the typical particle size of Kao-Cel/Co_3O_4 NC is 50 nm as shown in Fig. 5b. However, the average crystallite size of the NC calculated from the XRD data is 43 nm, which is in close agreement with the TEM acquired particle size (50 nm).

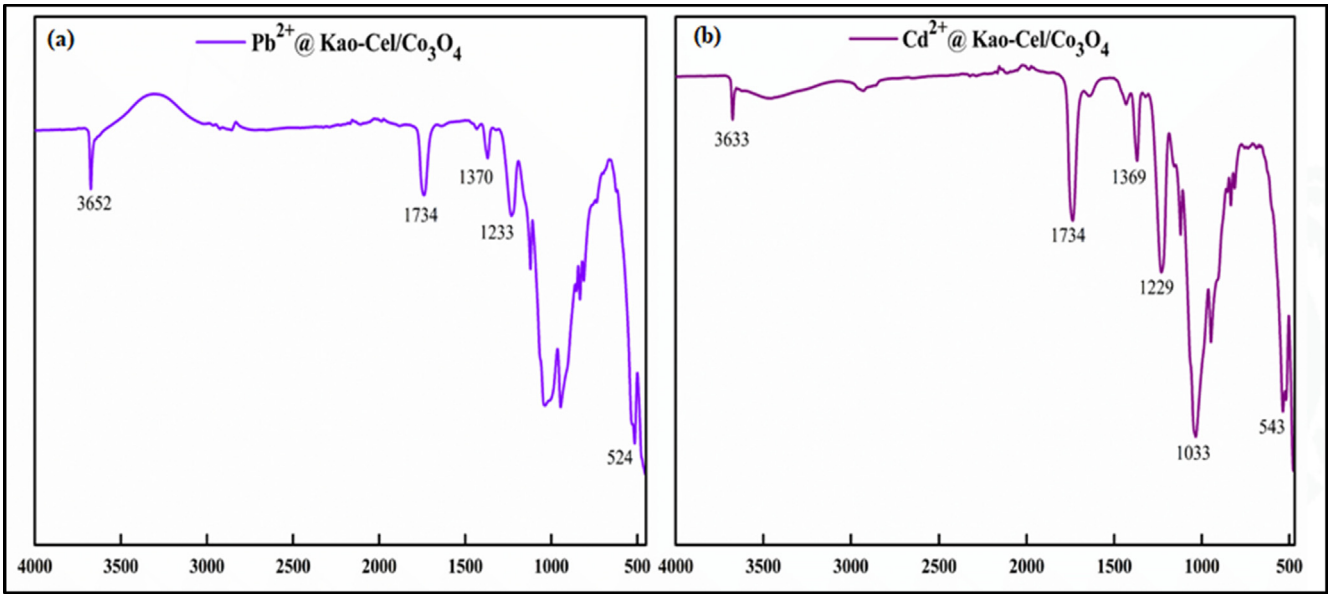

Fig. 2 FTIR spectra of Pb^{2+} and Cd^{2+} loaded Kao-Cel/Co_3O_4 nanocomposite.

3.2. Effect of adsorption variables on the uptake of Pb^{2+} and Cd^{2+} by Kao-Cel/Co_3O_4 nanocomposite

3.2.1. Variation in Kao-Cel/Co_3O_4 nanocomposite dose

In the adsorptive removal process, the quantity of adsorbed pollutants and removal efficiency are influenced by the adsorbent amount, therefore, optimization of adsorbent dosage is an important aspect that ensures usage of minimum adsorbent, which may regulate the overall operations cost in an efficient adsorption system. The effect of adsorbent mass for the removal competency of Pb^{2+} and Cd^{2+} was considered by varying the amount of Kao-Cel/Co_3O_4 NC from 0.4 to 2.4 g/L, and the results of the percentage removal of both the metal ions with change in adsorbent dosage are shown in Fig. 6a and 6b. The uptake effectiveness increases gradually up to 96.84% Pb^{2+} and 96.32% Cd^{2+} with an increment in the nanocomposite dose until 2.0 g/L where optimal uptake is observed. The rise in decontamination of Pb^{2+} and Cd^{2+} from the aqueous solution with an increase in adsorbent loading up to 2.0 g/L may be attributed to the increased number of available active adsorption sites. However, the removal efficiency presents a decreasing trait after that, which may either be due to a lesser number of accessible surface sites as a result of improved collision rate between nanocomposite particles, augmented active sites available for a fewer number of metal

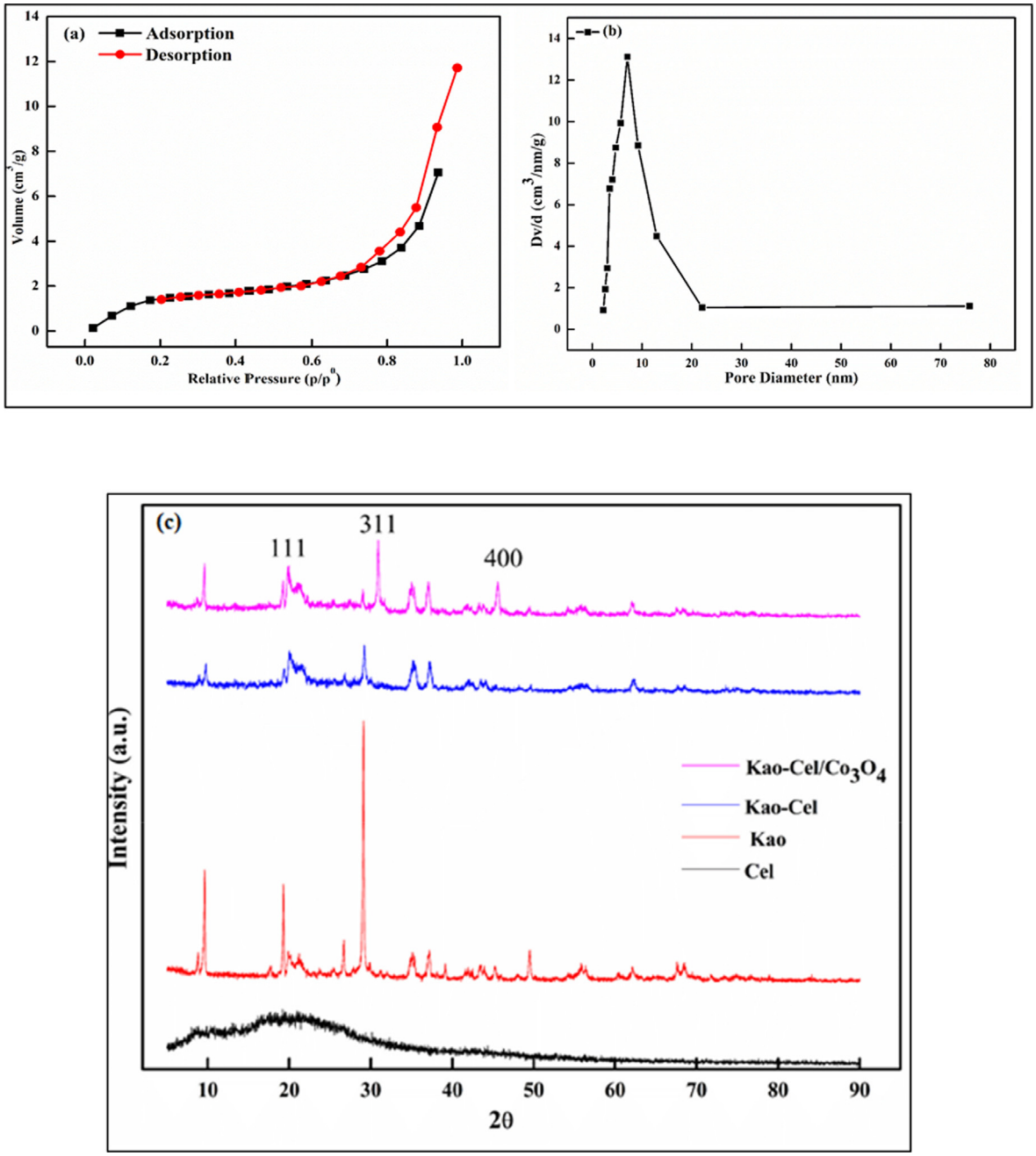

Fig. 3 N_2 adsorptions-desorption (a) and pore size (b), XRD spectra of Cel, Kao, Kao-Cel and Kao-Cel/Co_3O_4 nanocomposite (c).

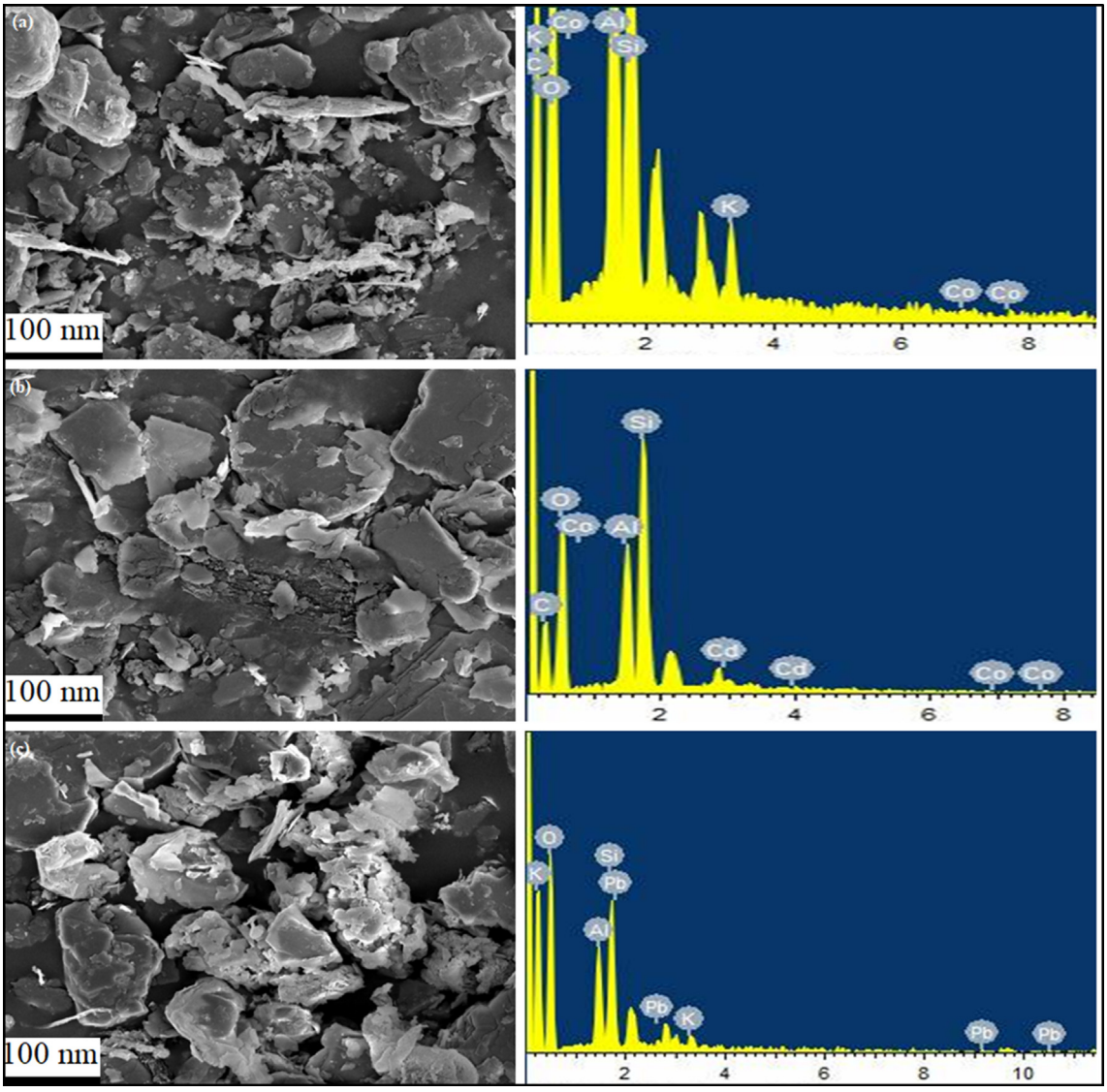

Fig. 4 SEM and EDX micrographs of (a) Kao-Cel/Co_3O_4 nanocomposite (b) Pb^{2+}, (c) Cd^{2+} loaded nanocomposite.

cations for adsorption or a drop in the overall surface area/or overlapping of surface-active sites, and an enhancement in the diffusional path length for the metal ions to grasp onto the adsorbent's surface (Khan et al., 2022). Hence, a 2.0 g/L adsorbent dosage was used for conducting the rest of the experiments. The Kao-Cel/Co_3O_4 NC illustrates an admirable adsorption aptitude in small dosage with good removal effectiveness. Similar results were accounted for by Huang et al. (Haung et al., 2020), and Tabesh et al. (Tabesh et al., 2018 for the adsorption of Pb^{2+} and Cd^{2+} onto CS/Cu_3(BTC)$_2$-SH nanocomposite and γ-Al_2O_3 nanoparticles.

3.2.2. Change in extraction time

The optimization of the residence time of adsorbate at the solid-solution interface delivers clue vis-à-vis the uptake rate and hence kinetics; the rapid equilibrium attainment leads to reduced overall treatment cost. The extraction time for the adsorptive elimination of Pb^{2+} and Cd^{2+} was studied by using the optimized adsorbent mass (2.0 g/L) and initial metals concentration (50 mg/L) in the range of 10–60 min. Fig. 6c and 6d illustrate that firstly the retrieval of metal ions gradually increases swiftly and then slowly till the equilibrium is achieved at 50 min when 96.75% Pb^{2+} and 95.30% Cd^{2+} are removed from the solution. The rapid capture by the Kao-Cel/Co_3O_4 NC at the initial stages of adsorption may be linked to the presence of abundant active reacting sites and high surface area, which gradually decreases with the progression of the process resulting in a slower uptake rate ultimately reaching a plateau corresponding to the saturation of vacant sites. Accordingly, for further studies, 50 min removal time is preferred. The swift confiscation time indicated that the fabricated nanocomposite is a promising scavenger for metal ions from the aquatic system. A similar outcome was detected for the adsorption of Pb^{2+} and Cd^{2+} onto modified and unmodified kaolinite and bifunctional magnetic mesoporous silica by Jiang et al. and Li et al. (Jiang et al., 2009; Li et al., 2021).

3.2.3. Alteration in the initial concentration of Pb^{2+} and Cd^{2+}

The initial contaminant molecules/ions concentration (C_i) is a significant operational variable as it governs the adsorption

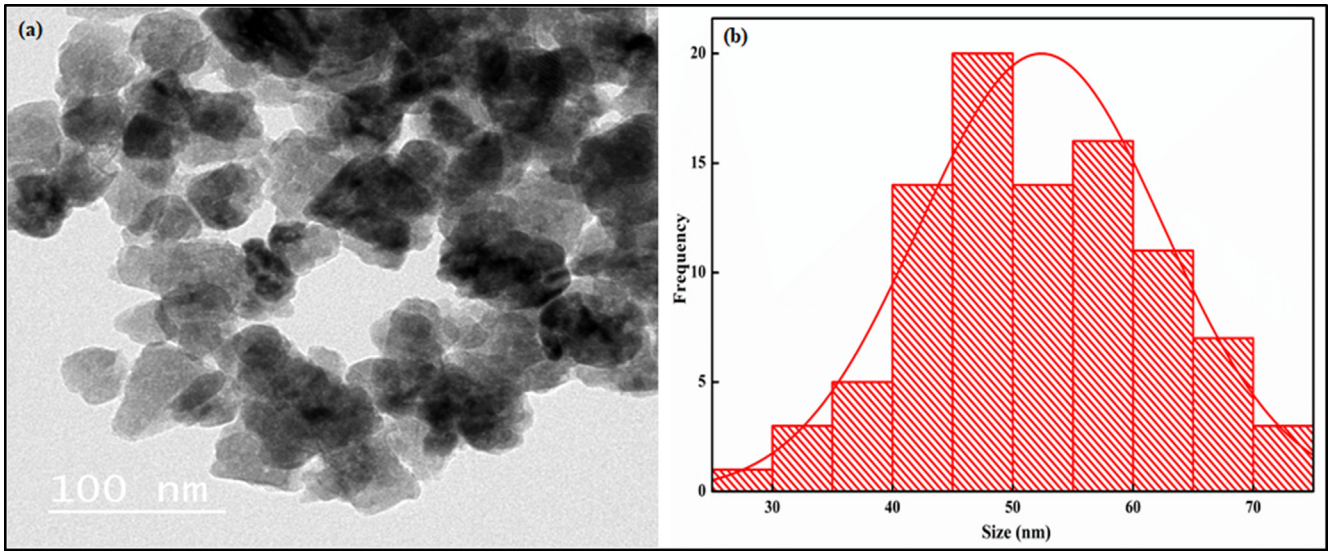

Fig. 5 TEM micrographs of (a) Kao-Cel/Co_3O_4 nanocomposite and (b) histogram (based on 95 particles).

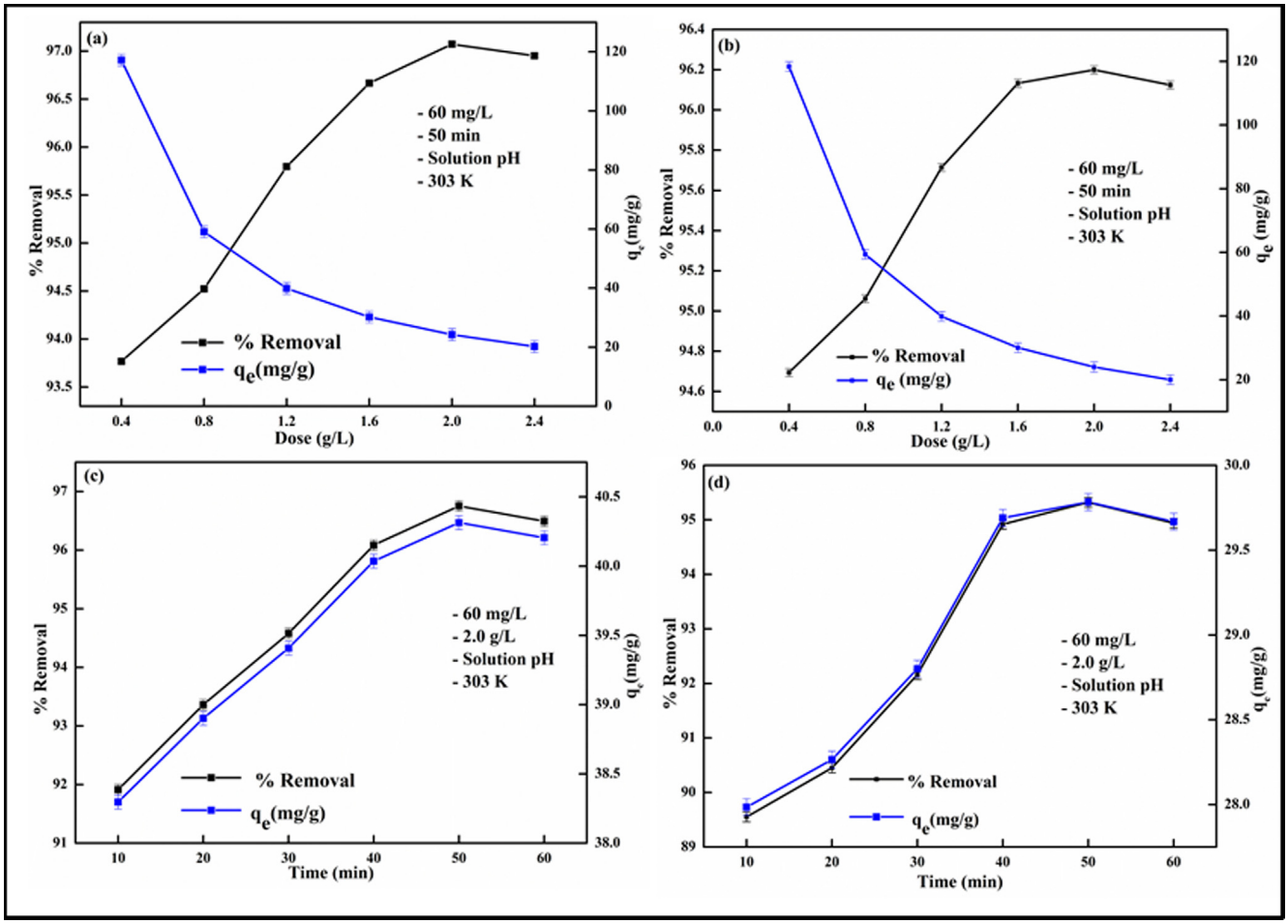

Fig. 6 Effect of adsorbent dose on (a) Pb^{2+}, (b) Cd^{2+} and contact time on (c) Pb^{2+}, (d) Cd^{2+} uptake.

competency of an adsorbent. The impact of C_i on the uptake ability of Kao-Cel/Co_3O_4 NC for the elimination of Pb^{2+} and Cd^{2+} was explored in C_i range of 20–80 mg/L with constant sorbent mass (2.0 g/L) for 50 min, and the results are displayed in Fig. 7a and 7b, respectively. As the C_i of M^{2+} (Pb^{2+} and Cd^{2+}) is increased from 20 to 60 mg/L, the aptitude of

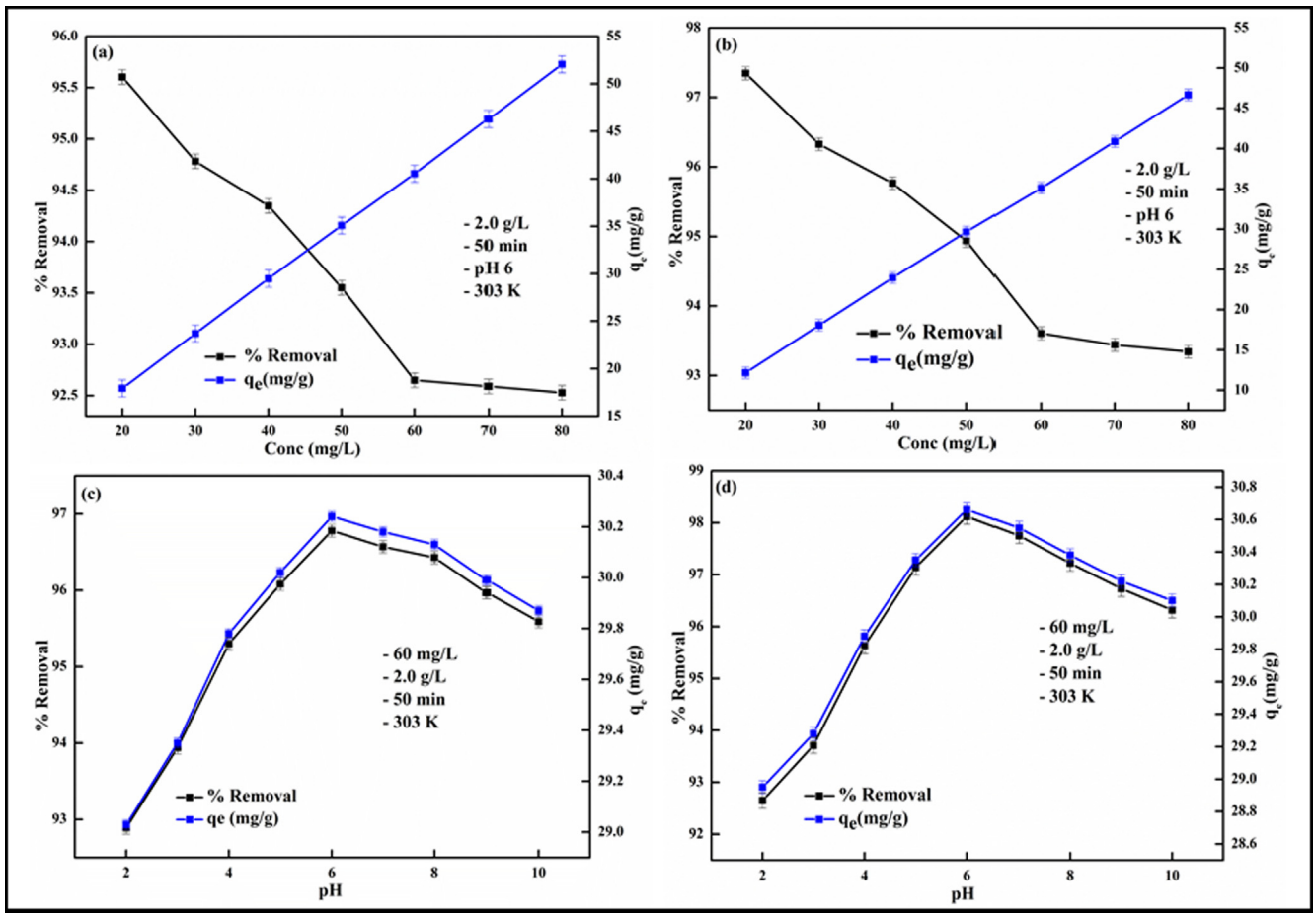

Fig. 7 Effect of initial concentration on (a) Pb^{2+}, (b) Cd^{2+} and effect of pH on Pb^{2+}, (d) Cd^{2+} removal.

adsorption decreases from 95.60 to 92.58% for Pb^{2+} and 97.34 to 93.34% for Cd^{2+}. A given amount of Kao-Cel/Co_3O_4 NC possesses a fixed number of surface binding sites. Initially, at lower M^{2+} concentration, the ratio of the adsorption sites to the number of M^{2+} ions are relatively high leading to boosted retention capacity. But as the Ci gradually increases, the available binding sites are progressively occupied by M^{2+} thus diminishing the adhering of M^{2+} onto fewer remaining active sites at higher C_i. However, only a slight change in adsorption behavior on further increasing the C_i beyond 60 mg/L is an indication of the saturation of sorbent binding sites. This suggests that a higher removal efficiency can be realized from the high concentration of liquid wastes by diluting the solution. Moreover, a rise in the adsorption capacity from 17.92–52.04 mg/g for Pb^{2+} and 12.16–46.67 mg/g for Cd^{2+} with an increment in C_i is due to the substantial driving force created by higher M^{2+} concentration exceeding the mass transfer resistance (Egbosiuba et al., 2022). These results are commensurate with Pb^{2+} and Cd^{2+} adsorption by chemically modified algal biomass and polyacrylamide/bentonite hydrogel nanocomposite (Khan et al., 2016; Khan et al., 2020).

3.2.4. Change in the initial solution pH

The adsorption capacity and the efficiency of the uptake process are essentially affected by the pH of the adsorbate solution as it not only influences the surface charge of the adsorbent but also the extent of ionization of the adsorbed molecules/ions. Hence, the adsorption of Pb^{2+} or Cd^{2+} from solution by Kao-Cel/ Co_3O_4 NC was explored by varying the initial pH of the working solutions between 2.0 and 10.0, adjusted with 0.1 M HCl or NaOH solution, at 303 K. The uptake efficacy of Pb^{2+} and Cd^{2+} by Kao-Cel/Co_3O_4 NC is revealed in Fig. 7c and 7d. A sharp increment in the sequestration efficacy for both metal cations is observed in the 2–6 pH range, which tends to decrease at pH > 8. Cadmium exists predominantly in the cationic forms as Cd^{2+} at pH up to 8.0, $Cd(OH)^+$, $Cd(OH)_2$ or $Cd(OH)_3^-$ at pH > 8.0–9.0, whereas lead is present as Pb^{2+} at pH < 6.0, $Pb(OH)^+$ at pH 7.0–9.0, $Pb(OH)_2$ at pH 9.0–11.0, and $Pb(OH)_3^-$ at pH > 11.0 (Khan et al., 2021). The adsorption behavior of Pb^{2+} and Cd^{2+} over the nanocomposite can be elucidated based on the pH_{zpc} of the adsorbent (4.5). This endorses that the NC surface charge is positive at pH < pH_{zpc} and negative at pH > pH_{zpc}, thus favoring the adsorption of negative species of both Pb^{2+} or Cd^{2+} ions at pH < pH_{zpc} and the positive species at pH > pH_{zpc} involving electrostatic interactions. With a lower operating pH, the Pb^{2+} or Cd^{2+} and H_3O^+ vie for each other for the adsorption sites, and probably the adsorption onto the Kao-Cel/Co_3O_4 NC surface occurs via an ion exchange procedure between Pb^{2+}/Cd^{2+} and H_3O^+. However, with an increase in pH, the dominant species such as Pb^{2+}, $Pb(OH)^+$/Cd^{2+}, $Cd(OH)^+$ experience an increasing electrostatic

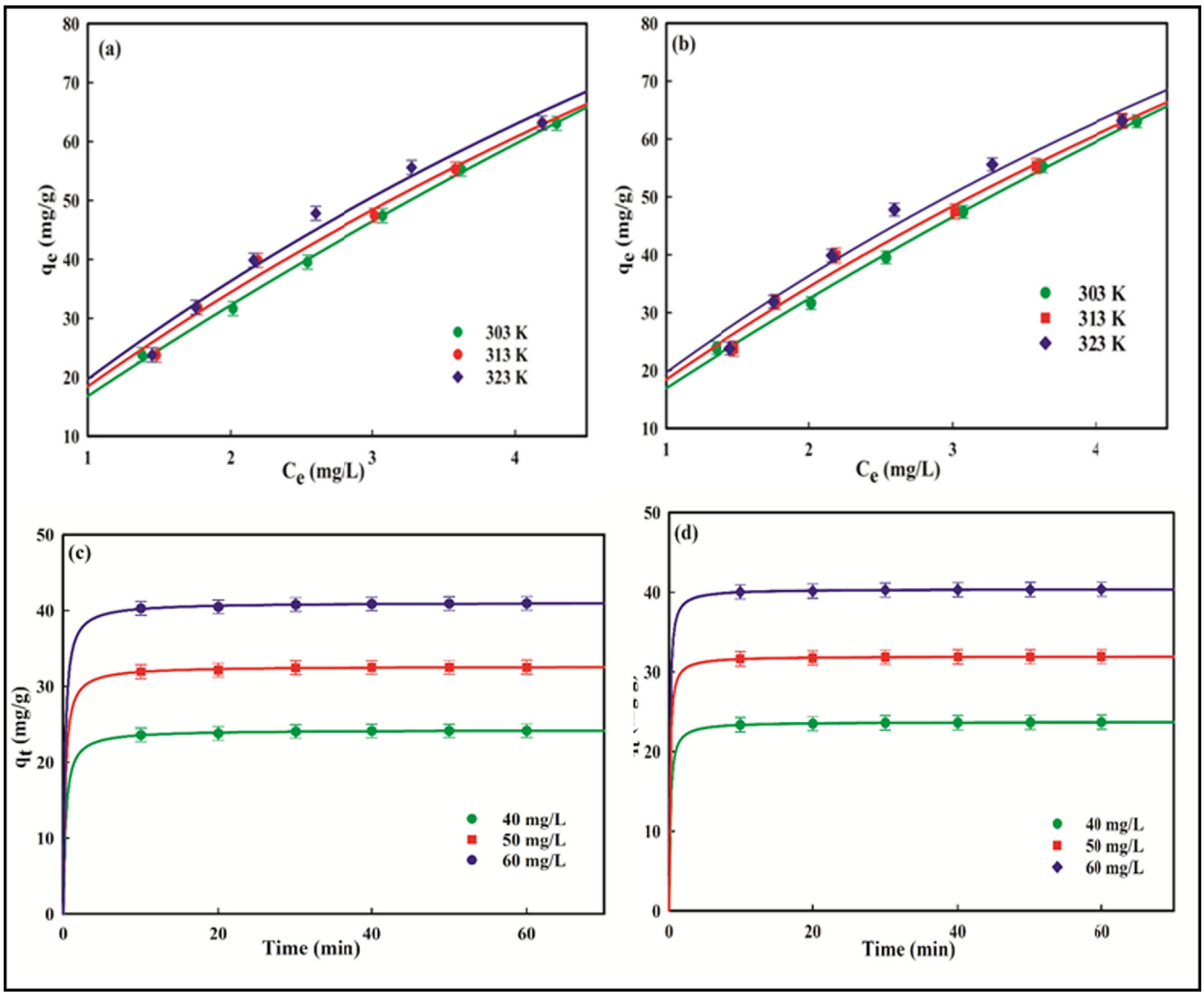

Fig. 8 Langmuir isotherm plots for (a) Pb^{2+}, (b) Cd^{2+}, and pseudo-second order kinetic plots for (c) Pb^{2+}, (d) Cd^{2+} adsorption.

attraction leading to elevated adsorption accounting for up to 96.78% Pb^{2+} and 98.12% Cd^{2+} removal efficiency at pH 6.0. With the further rise in the solution pH, the adsorption efficiency tends to diminish probably due to electrostatic repulsion faced by the negatively charged species and/or precipitation of metal hydroxides. Soltani et al. (Soltani et al., 2018) and Ahmad et al. (Ahmad and Haseeb, 2015), depicted similar results for adsorptive behavior of Pb^{2+} and Cd^{2+} onto poly(vinyl alcohol) and amino-modified MCM-41 and groundnut husk modified with guar gum. Thus, the maximal removal efficiency is attained at pH 6.0. Similar pH_{max} values of 6 have been reported in the literature for optimal removal of Cd^{2+} and Pb^{2+} onto bentonite-chitosan composite (Sellaoui et al., 2018 and poly(acrylic acid)/nano sorbent (Bhatia et al., 2017).

3.3. Analysis of the adsorption isotherm data

Langmuir's model supposes that on the sorbent surface there is no saturated atomic force field, and once the sorbent surface is covered by sorbate molecules, the force field gets saturated and no further adsorption can occur, which corresponds to monolayer adsorption (Langmuir, 1918). From the slope and intercept of the plot of the quantity of Pb^{2+}/Cd^{2+} adsorbed at equilibrium (q_e) as a function of solute's equilibrium concentration in bulk phase (C_e), shown in Fig. 8a and b, the values of Langmuir saturation capacity, Q_m and Langmuir adsorption energy, b_L was determined. The deduced values of Q_m (mg/g), b_L (L/mol), R^2 and separation factor, R_L ($=\frac{1}{1+bC_0}$) are summarized in Table 1. The Q_m values (in mg/g) for the confiscation of Pb^{2+} and Cd^{2+} at 303 K, 313 K, and 323 K are in the 155.78–293.68 and 132.35–267.85 range, respectively. This increasing trend in the Q_m values may probably be a consequence of the rise in temperature providing the energy needed for the higher mobility of adsorbate ions across the external layer for enhanced interaction with the surface sites, and/or an increased rate of diffusion into the interior pores, which is the characteristic of the endothermic removal process. The maximum removal capacities of Kao-Cel/Co_3O_4 NC are 293.68 mg Pb^{2+}/g and 267.85 mg Cd^{2+}/g, respectively at

Table 4 Adsorption thermodynamic parameters.

	Conc (mg/L)	ΔH^o (kJ/mol)	ΔS^o (kJ/mol/K)	ΔG^o (kJ/mol)			
				303 K	313 K	323 K	333 K
Pb^{2+}	50	3.98	0.038	−7.83	−8.22	−8.61	−9.00
Cd^{2+}	50	6.991	0.049	−7.86	−8.35	−8.84	−9.33

323 K. The magnitude of Q_m is of interest to many researchers in establishing the adsorption competence of different adsorbents. But the direct comparison of Q_m may not always lead to unequivocal conclusions because of differing optimal experimental conditions. A comparative account of Q_m of the present adsorbent with those of other adsorbents along with experimental conditions is summarized in Table 2. The Q_m of Kao-Cel/Co_3O_4 NC for Pb^{2+}/Cd^{2+} are considerably higher than other stated adsorbents (Table 2), which propounds its superior adsorption performance.

Freundlich's model describes that the surface of the sorbent is heterogeneous with a continuous dispersal of active sites, and the adsorption is multi-layered (Freundlich, 1906). The values of the Freundlich adsorption efficiency, K_F, and Freundlich isotherm constant, $1/n_F$, R^2, and *SEE*, computed from the q_e versus C_e plot (Fig. S2), are given in Table 1. The gradual increase in K_F {(mg/g)(mg/ L)$^{1/n}$} from 17.48–20.52 for Pb^{2+} and 17.01–18.67 for Cd^{2+} with change in temperature from 303 to 323 K substantiates the endothermic adsorption phenomenon and better adsorption performance at elevated temperature. The Freundlich parameter, n_F is used to authenticate whether the adsorption is linear (n = 1), physical and favorable (n_F > 1) or chemical (n_F < 1), and further explicates the deviation from the linear adsorption (Della Puppa et al., 2013). Its values greater than unity (Pb^{2+} = 1.23–1.13; Cd^{2+} = 1.91–1.96) highlight the favorable and physical uptake process. The parameter, $1/n_F$ is a measure of the surface heterogeneity, its value approaching nearer to zero dictates a more heterogeneous surface. The values (Pb^{2+} = 0.813–0.885; Cd^{2+} = 0.523–0.511) proposes low to moderate surface heterogeneity.

Temkin adsorption model describes the interaction between sorbent and sorbate, which explore the heat of adsorption in term of temperature in layers assuming that the heat of adsorption decreases with the degree of the adsorption process (Temkin, 1940). The model equation (Table 1) is generally used to estimate the equilibrium binding constant, K_T (L/g), and the heat of adsorption, b_T (=RT/β_T) (kJ/mol) from q_e versus C_e curve (Fig. S3) for the adsorption process. The calculated values of these parameters along with R^2 and *SEE* are depicted in Table 1. The positive values of b_T (0.074–0.071 kJ/mol for Pb^{2+} and 0.199–0.183 kJ/mol for Cd^{2+}) at all studied temperatures provide for favorable physical and endothermic adsorption. Only a slight variation in K_T (Table 2) reflects that the binding energy is not much influenced by the changing temperature.

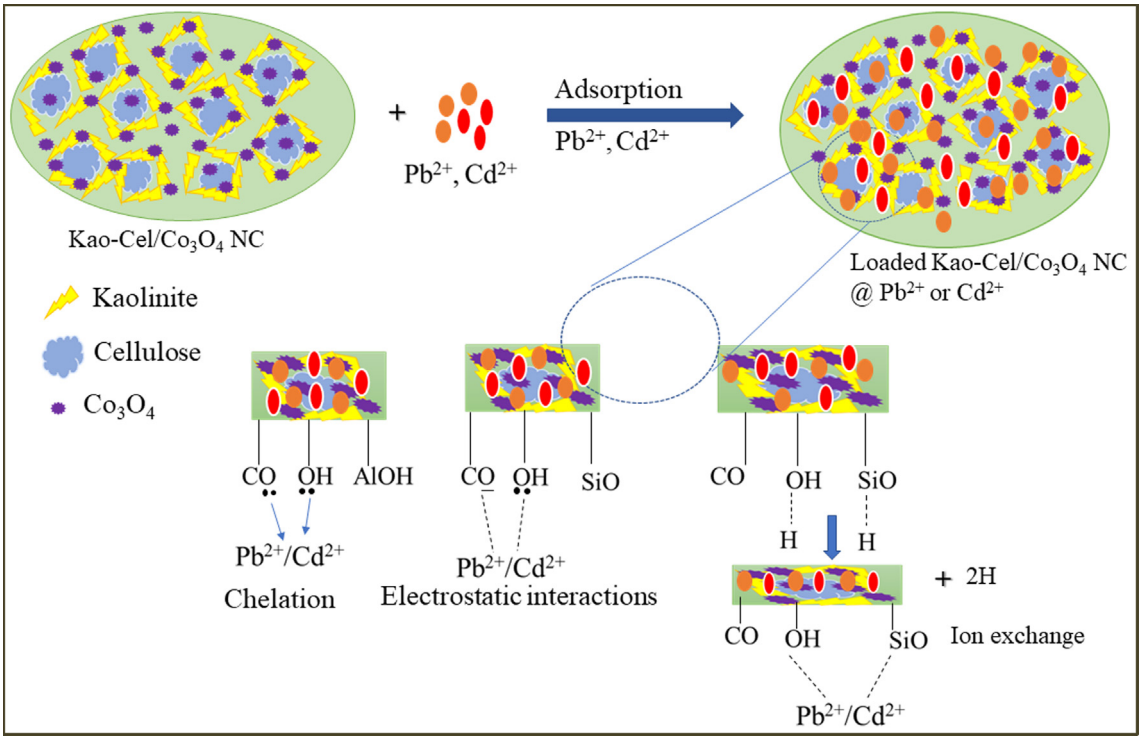

Fig. 9 Plausible interaction mechanism of Pb^{2+}/Cd^{2+} with Kao-Cel/Co_3O_4 nanocomposite surface.

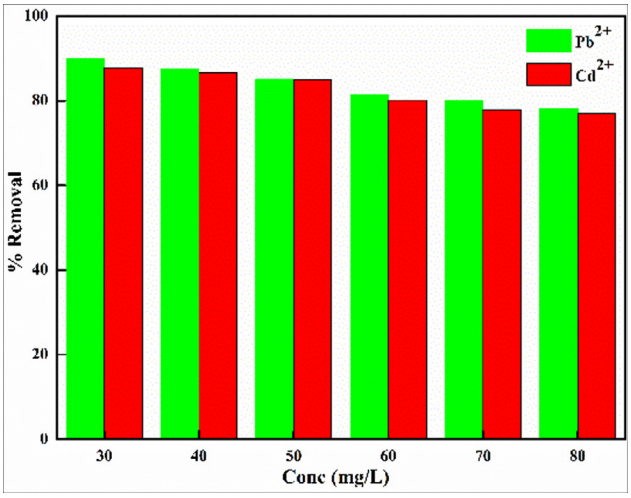

Fig. 10 Effect of real wastewater on the removal efficiency of Kao-Cel/Co_3O_4 nanocomposite.

D-R isotherm model usually envisages the nature of sorbate adsorption over the surface of sorbent (physisorption or chemisorption), and also examines both homogeneous and heterogeneous adsorption (Dubinin and Radushkevich, 1947). The D–R model constants, q_D (mg/g) related to the degree of adsorbate adsorption and K_D (mol^2/kJ^2) associated with the average adsorption energy per mole, evaluated from the q_e versus C_e isotherm plot (Fig. S4) together with R^2 and *SEE*, is provided in Table 1. The probable energy of adsorption, $E\ (= \frac{1}{(2B_D)^{1/2}})$, which is used to extricate physical or chemical adsorption mechanism was estimated from K_D $(= B_D R^2 T^2)$. The increase in the estimated q_D values (mg/g) for Pb^{2+} (117.09–121.83) and Cd^{2+} (117.24–120.81) with elevation in temperature elucidates a high extent of adsorption capacity at higher temperature. Less than 8.0 kJ/mol values of *E* for Pb^{2+} (0.34–0.31 kJ/mol) and Cd^{2+} (0.35–0.31 kJ/mol) entitles physical sorption.

To comprehend the most fitted isotherm model, the higher R^2 and lower *SEE* parameters are generally considered. From the results in Table 1, it is concluded that the Langmuir model presents a higher R^2 (0.998–0.989 for Pb^{2+} and 0.996–0.985 for Cd^{2+}) and lower *SEE* (0.340–0.260 for Pb^{2+} and 0.682–0.296 for Cd^{2+}) values relative to rest of the models signifying that Langmuir isotherm best explain the equilibrium data. The adsorption process of Pb^{2+}/Cd^{2+} ions, therefore, is believed to be a homogenous monolayer onto the surface of Kao-Cel/Co_3O_4 NC in accordance with the Langmuir model.

3.4. Evaluation of the adsorption kinetics data

The rate constants for pseudo-first order (k_1; 1/min), pseudo-second order (k_2; g/mg/min) and q_e (mg/g) were calculated from the respective kinetic plots of q_t against *t* (Fig. S5) and (Fig. 8c and 8d), respectively. The determined values of k_1, k_2, and other related parameters at three different initial concentrations (C_i = 40, 50, and 60 mg/L) are given in Table 3. The best-fitted kinetic model was evaluated based on R^2 and *SEE* values. The pseudo-second order model with close to unity values of R^2 (Pb^{2+}: 0.975–0.978; Cd^{2+}: 0.971–0.919) and lower *SEE* (Pb^{2+}: 0.033–0.018; Cd^{2+}: 0.061–0.082) for all Ci stipulates that this model most appropriately describes the kinetic data in comparison with pseudo-first order kinetics. The best fitting of kinetic data by the pseudo-second order model illustrates that the sorption mechanism depends on the adsorbent and adsorbate, and chemisorption and/or physicochemical interactions between species on the surface may be rate-limiting (Abd El Aal et al., 2019). The k_2, which represents the adsorbate's affinity for the adsorbent surface (Della Puppa et al., 2013) is higher for Pb^{2+} (0.250–0.241 g/mg/min) in comparison to that of Cd^{2+} (0.136–0.115 g/mg/min), indicating a greater affinity of Pb for Kao-Cel/Co_3O_4 NC. A similar result of greater affinity of Pb^{2+} for diatomite has been explained based on its capability to occupy both the interlayer and surface edge sites (Wan Ngah et al., 2011).

The adsorptive uptake rate of M^{2+} ions usually depend on external liquid film diffusion or intraparticle diffusion of solute or a combination of both these steps. So, to gain further acuity into the mechanism and to clarify the rate-dominating steps impacting the adsorption kinetics, the data was scrutinized by intra-particle diffusion and liquid-film diffusion models. The Weber-Morris intra-particle diffusion model assumes the probable transportation of the dissolved pollutants (Pb^{2+}/Cd^{2+}) from the aqueous system onto the solid adsorbent as a function of the intra-particle conveyance mechanism, while the Boyd liquid-film diffusion model considers the transfer of adsorbate molecules/ions through a liquid film encompassing the adsorbent. The extent to which the adsorption data fit the models is predicted by the linear plot of q_t versus $t^{0.5}$ (Fig. S6) and $\ln(1 - q_t/q_e)$ versus *t* (Fig. S7). The values of intra-particle diffusion constant, k_i (mg/g $min^{0.5}$), liquid film diffusion rate constant, k_A (1/min), intercept that is associated closely with the thickness of the boundary layer, C_i, $R^{2\prime}$ and *SEE* for Pb^{2+} and Cd^{2+} are presented in Table 3. The

Table 5 Adsorption-desorption cycles.

Regeneration cycles	Adsorption (%) Pb^{2+}	Desorption (%) Pb^{2+}	Adsorption (%) Cd^{2+}	Desorption (%) Cd^{2+}
1.	94.96	96.08	94.87	97.14
2.	90.67	94.81	90.34	94.34
3.	87.21	91.07	89.41	90.89
4.	81.28	88.72	86.79	86.93
5.	77.99	84.31	72.93	83.02

intra-particle diffusion plot (Fig. S6) reveals that adsorption of Pb^{2+} and Cd^{2+} is not linear over the studied concentration range, and no straight-line curve passes through the origin. because the curves do not pass through the origin shows. Hence, the accomplishment of the Pb^{2+}/Cd^{2+} adsorption onto Kao-Cel/Co_3O_4 NC is not solely controlled by the intra-particle diffusion mechanism. Similarly, the straight-line curves based on the liquid-film diffusion model with a non-zero intercept recommend that the Pb^{2+}/Cd^{2+} diffusion through the liquid-film is not the solitary rate-controlling step. The values of C_{ip} for Pb^{2+} and Cd^{2+} at 40–50 mg/L are 31.43–39.83, and 31.60–39.83, respectively. The higher C_{ip} demonstrates a greater boundary layer effect, and consequently liquid-film diffusion as the dominant rate-controlling factor. The observed enhancement in C_{ip} with an increase in initial Pb^{2+} and Cd^{2+} concentration reflects that the boundary layer effect is more pronounced at higher initial sorbate concentration. It may, therefore, be proposed that the adsorption mechanism is not confined merely to intra-particle and liquid-film diffusion but is controlled by numerous other operating mechanisms.

3.5. Thermodynamic studies

The adsorption thermodynamic parameters were evaluated at four temperatures (303, 313, 323, and 333 K). Adsorption of a solute at a solid-solution interface, in general, is accompanied by negative free energy change (ΔG°), which is suggestive of the spontaneity of the process. The positive entropy (ΔS°) and enthalpy change (ΔH°) attribute to an increase in randomness of displaced water molecules from a solid surface due to the gain of translational entropy, and endothermic adsorption. The negative values of entropy and enthalpy changes, however, impute a decrease in translational entropy as a result of regular attachment/association of water molecules and adsorbate fixation or immobilization onto the adsorbent surface, and the exothermic nature of the adsorbent. The negative ΔG° (in kJ/mol) at four studied temperatures (between −7.83 to −9.00 for Pb^{2+}; −7.86 to −9.33 for Cd^{2+}), and positive ΔH° (Pb^{2+}: 3.98 kJ/mol; Cd^{2+}: 6.99 kJ/mol) and ΔS° (Pb^{2+}: 0.038 kJ/mol/K; Cd^{2+}: 0.049 kJ/mol/K), depicted in Table 4, advocate that the adsorption of Pb^{2+} and Cd^{2+} onto Kao-Cel/Co_3O_4 NC is spontaneous, feasible and endothermic (Fig. S8). An increment in the ΔG° with increasing temperature from 303 K to 333 K illustrates more preferred adsorption at higher temperature. The values ΔG° are well within the range (zero and −20 kJ/mol) for the physisorption mechanism, which is further supported by the ΔH° values (3.68 and 6.99 kJ/mol) in the 2.1–20.9 kJ/mol range in accordance with physisorption involving van der Waals interactions and hydrogen bonding. The positive ΔS° values (0.038–0.049 kJ/mol/K) foresee a slight enhancement in the randomness at the interface between two phases probably due to displaced water molecules gathering more translational entropy. However, the low ΔS° values point to no significant change in entropy.

3.6. Adsorption mechanism

Generally, the adsorption of metal ions onto clay-based nanocomposite occurs through electrostatic interactions and ion exchange mechanisms between the contaminants and biosorbent. The functional groups of the Kao-Cel/Co_3O_4 NC can act as active sites for metal ions sorption. The solution pH influences the mechanism of ion exchange which is prevalent between Pb^{2+}/Cd^{2+} and Si^{2+} of the Kaolinite phase. Also, the increase in H^+ ions in an acidic medium competes with positively charged contaminants (Pb^{2+} and Cd^{2+}) leading them to be adsorbed onto the surface of Kao-Cel/Co_3O_4 NC (Iqbal et al., 2009) validates the involvement of electrostatic attraction (physical adsorption). The FTIR studies display the weakening and shifting of the O—H and C═O/C—O bands at 952 and 1040 cm^{-1} confirming the formation of the coordinated —OH and C═O/CO— metal ion complexes. Moreover, the change of the absorption band at 952 cm^{-1} assigned to stretching vibration of —OH deformations of the inner surface hydroxyl group of kaolinite is the indication that —OH groups are involved in binding to metals ions, which is in accordance with previously reported works (Irani et al., 2015) between metals ions and the functional groups on the adsorbent surface. Therefore, the adsorption of Pb^{2+} and Cd^{2+} onto Kao-Cel/Co_3O_4 NC might be due to the combined effect of electrostatic, ion-exchange, and chelation mechanisms respectively. The plausible mechanisms of Pb^{2+} and Cd^{2+} sequestration onto the Kao-Cel/Co_3O_4 NC are schematically demonstrated in Fig. 9.

3.7. Desorption of Pb^{2+} and Cd^{2+}

To elucidate the practical utility and adsorption mechanism of Kao-Cel/Co_3O_4 NC, desorption studies were performed. If the sorbed M^{2+} ions show water-induced desorption, it can be inferred that the attachment of metal ions onto the adsorbent surface involves weak interactive forces or bonds. However, if desorption is achieved with a strong base or acid (NaOH/HCl) then the adsorption of M^{2+} ions onto the adsorbent surface may include electrostatic attraction or ion exchange (Baskar et al., 2022). After the fifth adsorption/desorption cycle, 84.31% and 83.02% desorption and 77.99% and 72.93% adsorption occur for Pb^{2+} and Cd^{2+}, respectively (Table 5) indicating the excellent regeneration property of the Kao-Cel/Co_3O_4 NC adsorbent.

3.8. Removal efficiency for metal ions from real wastewater sample spiked with Pb^{2+}/Cd^{2+}

Under optimized conditions, the %removal is reduced from 90.86–83.17 for Pb^{2+} and 87.75–76.93 for Cd^{2+} with increment of initial concentrations (Fig. 10). The decrease in the removal efficacy may be due to the presence of different contaminants in the real source, which interferes with the uptake of both metal ions. However, the decrease is not so obvious that recommends that Kao-Cel/Co_3O_4 NC can be used effectively for Pb^{2+} and Cd^{2+} removal from the real wastewater.

3.9. Disposal of the spent adsorbent

The sustainable management of the exhausted adsorbents is one of the major tasks in the adsorption-based treatment system. Their disposal through landfills, regeneration by desorption process for use (ceramics, catalyst/catalyst support, capacitor)/reuse and recycle, and ultimately incineration are viable strategies adopted for managing the spent adsorbents .

However, the present adsorbent poses no disposal issues because of its green characteristics, and good regeneration potential and recyclability.

4. Conclusions

The Kao-Cel/Co_3O_4 nanocomposite has been fabricated via a green approach by supporting kaolinite-cellulose by green Co_3O_4 nanoparticles using *Berberis lycium* leaf extract, characterized by FTIR, XRD, BET, SEM-EDX and TEM studies, and utilized as an eco-friendly adsorbent for the amputation of Pb^{2+} and Cd^{2+} from the aquatic system. The BET surface area of Kao-Cel/Co_3O_4 NC is 85.92 m^2/g, pore size determined by BJH is about 0.024 cm^3/g and a pore diameter is 7.221 nm. The pore diameter in the 2–50 nm range specifies the mesoporous characteristics of the adsorbent. Various parameters affecting the adsorption such as dosage (2.0 g/L), agitation time (50 min), initial Pb^{2+} and Cd^{2+} ions concentration (60 mg/L), pH (6), are appraised for sequestration of Pb^{2+} and Cd^{2+}. Adsorption data is best explained by the Langmuir model, which indicates the monolayer adsorption of M^{2+} ions onto homogenous surface sites of Kao-Cel/ Co_3O_4 NC. The calculated maximum saturation capacity, Q_m is 293.67 mg Pb^{2+}/g and 267.84 mg Cd^{2+}/g, which displays much better efficacy of Kao-Cel/Co_3O_4 NC relative to most other existing adsorbents. Pseudo-second order kinetics governs the adsorption process of Pb^{2+} and Cd^{2+} onto Kao-Cel/Co_3O_4 NC. The overall thermodynamic spontaneity, feasibility, and endothermic nature of adsorption were evaluated. An increase in the randomness at the solid-solution interface is indicated by positive ΔS° values during adsorption. Real water analysis depicted a minor decrease in removal efficiency indicating potential of Kao-Cel/Co_3O_4 for practical purposes. The Kao-Cel/Co_3O_4 NC can be applied effectively for the removal of Pb^{2+} and Cd^{2+} for five cycles without much loss in efficacy. The present study explicitly establishes the as-synthesized nanocomposite as a proficient and excellent adsorbent for confiscation of hazardous metal ions from the wastewaters.

CRediT authorship contribution statement

Daud Hussain: Conceptualization, Writing – original draft, Methodology, Investigation, Data curation, Formal analysis. **Suhail Ayoub Khan:** Investigation, Data curation, Software, Formal analysis; Writing – review & editing. **Salman S Alharthi:** Validation, Writing – review & editing, Resources. **Tabrez Alam Khan:** Validation, Writing – review & editing, Resources, Supervision.

Declaration of Competing Interest

The authors declare that they have no known competing financial interests or personal relationships that could have appeared to influence the work reported in this paper.

Acknowledgement

The author (DH) thanks the Ministry of Tribal Affairs, Govt. of India for the award of Senior Research Fellowship. The author from Taif University (SSA) acknowledges the financial support through Taif University Researchers Supporting Project number (TURSP-2020/90), Taif University, Taif, Saudi Arabia.

Appendix A. Supplementary material

Supplementary data to this article can be found online at https://doi.org/10.1016/j.arabjc.2022.103925.

References

Abd El Aal, S.A., Abdelhady, A.M., Mansour, N.A., Hassan, N.M., Elbaz, F., Elmaghraby, E.K., 2019. Physical and chemical characteristics of hematite nanoparticles prepared using microwave-assisted synthesis and its application as adsorbent for Cu, Ni Co, Cd and Pb from aqueous solution. Mater. Chem. Phys. 235, 121771.

Abunah, D., Onindo, C., Andala, D., Ochoti, E., 2019. Physico-chemical removal of heavy metals from contaminated water using recyclable montmorillonite cellulose nanocomposite. J. Mater. Environ. Sci. 10, 1349–1361.

Adebowale, K.O., Unuabonah, I.E., Olu-Owolabi, B.I., 2006. The effect of some operating variables on the adsorption of lead and cadmium ions on kaolinite clay. J. Hazard. Mater. 134, 130–139.

Ahmad, R., Haseeb, S., 2015. Absorptive removal of Pb^{2+}, Cu^{2+} and Ni^{2+} from the aqueous solution by using groundnut husk modified with guar gum (GG): Kinetic and thermodynamic studies. Groundw. Sustain. Dev. 1, 41–49.

Ajala, O.J., Khadir, A., Ighalo, J.O., Umenweke, G.C., 2022. Cellulose-based nano-biosorbents in water purification in "Nano-biosorbents for decontamination of water, air, and soil pollution", Chapter 17, pp. 395-415.

Akter, M., Bhattacharjee, M., Dhar, A.K., Rahman, F.B.A., Haque, S., Rashid, T.U., Kabir, S.M.F., 2021. Cellulose-based hydrogels for wastewater treatment: A concise review. Gels 7, 30.

Ali, S., Khatri, Z., Oh, K.W., Kim, I.-S., Kim, S.H., 2014. Zein/cellulose acetate hybrid nanofibers: Electrospinning and characterization. Macromol. Res. 22, 971–977.

Awokoya, K.N., Oninla, V.O., Bello, D.J., 2021. Synthesis of oxidized *Dioscorea dumentorum* starch nanoparticles for the adsorption of lead(II) and cadmium(II) ions from wastewater. J. Clean. Prod. 15, 100440.

Baskar, A.V., Bolan, N., Hoang, S.A., Sooriyakumar, P., Kumar, M., Singh, L., Jasemizad, T., Padhye, L.P., Singh, G., Vinu, A., Sarkar, B., Kirkham, M.B., Rinklebe, J., Wang, S., Wang, H., Balasubramanian, R., Siddique, K.H.M., 2022. Recovery, regeneration and sustainable management of spent adsorbents from wastewater treatment streams: A review. Sci. Total Environ. 822, 153555.

Bhatia, M., Rajulapati, S.B., Sonawane, S., Girdhar, A., 2017. Synthesis and implication of novel poly(acrylic acid)/nanosorbent embedded hydrogel composite for lead ion removal. Sci. Rep. 7, 16413.

Boyd, G.E., Adamson, A.W., Myers Jr., L.S., 1947. The exchange adsorption of ions from aqueous solutions by organic zeolites. II. Kinetics. J. Am. Chem. Soc. 69, 2836–2848.

Cai, J., Lei, M., Zhang, Q., He, J.-R., Chen, T., Liu, S., Fu, S.-H., Li, T.-T., Liu, G., Fei, P., 2017. Electrospun composite nanofiber mats of Cellulose@Organically modified montmorillonite for heavy metal ion removal: Design, characterization, evaluation of absorption performance. Composites. Part A Appl. Sci. Manuf. 92, 10–16.

Cheng, S., Liu, Y., Xing, B., Qin, X., Zhang, C., Xia, H., 2021. Lead and cadmium clean removal from wastewater by sustainable biochar derived from poplar saw dust. J. Clean. Prod. 314, 128074.

Chi, T., Zuo, J., Liu, F., 2017. Performance and mechanism for cadmium and lead adsorption from water and soil by corn straw biochar. Front. Environ. Sci. Eng. 11, 1–8.

Del Mar Orta, M., Martín, J., Santos, J.L., Aparicio, I., Medina-Carrasco, S., Alonso, E., 2020. Biopolymer-clay nanocomposites as novel and ecofriendly adsorbents for environmental remediation. Appl. Clay Sci. 198, 105838.

Della Puppa, L., Komárek, M., Bordas, F., Bollinger, J.C., Joussein, E., 2013. Adsorption of copper, cadmium, lead and zinc onto a synthetic manganese oxide. J. Colloid Interface Sci. 399, 99–106.

Dubinin, M.M., Radushkevich, L.V., 1947. Equation of the characteristic curve of activated charcoal. Proc. Acad. Sci. Phys. Chem. URSS. 55, 331–333.

Egbosiuba, T.C., Egwunyenga, M.C., Tijani, J.O., Mustapha, S., Abdulkareem, A.S., Kovo, A.S., Lisak, G., 2022. Activated multi-walled carbon nanotubes decorated with zero valent nickel nanoparticles for arsenic, cadmium and lead adsorption from wastewater in a batch and continuous flow modes. J. Hazard. Mater. 423, 126993.

España, V.A.A., Sarkar, B., Biswas, B., Rusmin, R., Naidu, R., 2019. Environmental applications of thermally modified and acid activated clay minerals: current status of the art. Environ. Technol. Innov. 13, 383–397.

Fard, E.M., Parvareh, A., Moravaji, M.K., 2022. Optimization of removal of lead and cadmium from industrial wastewater by ethylenediamine-modified single-walled carbon nanotubes. Int. J. Environ. Sci. Technol. 19, 2747–2760.

Farhadi, S., Javanmard, M., Nadri, G., 2016. Characterization of cobalt oxide nanoparticles prepared by the thermal decomposition. Acta Chim. Slov. 63, 335–343.

Flora, G., Gupta, D., Tiwari, A., 2012. Toxicity of lead: a review with recent updates. Interdiscip. Toxicol. 5, 47–58.

Freundlich, H., 1906. Over the adsorption in solution. J. Phys. Chem. 57, 385–471.

Gu, S., Kang, X., Wang, L., Lichtfouse, E., Wang, C., 2019. Clay mineral adsorbents for heavy metal removal from wastewater: a review. Environ. Chem. Lett. 17, 629–654.

Ho, Y.S., McKay, G., 2003. Sorption of dyes and copper onto biosorbents. Process Biochem. 38, 1047–1061.

Hua, R., Li, Z., 2014. Sulfhydryl functionalized hydrogel with magnetism: Synthesis, characterization, and adsorption behavior study for heavy metal removal. Chem. Eng. J. 249, 189–200.

Huang, L., Huang, W., Shen, R., Shuai, Q., 2020. Chitosan/thiol functionalized metal–organic framework composite for the simultaneous determination of lead and cadmium ions in food samples. Food Chem. 330, 127212.

Huang, Y., Zhao, R., Liu, W., Li, Y., Zhang, P., Wang, S., Wang, L., 2018. Using pretreated chestnut endothelium to adsorb lead and cadmium ions from water. Saudi J. Biol. Sci. 25, 1154–1162.

Iqbal, M., Schiewer, S., Cameron, R., 2009. Mechanistic elucidation and evaluation of biosorption of metal ions by grapefruit peel using FTIR spectroscopy, kinetics and isotherms modeling, cations displacement and EDX analysis. J. Chem. Technol. Biotechnol. 84, 1516–1526.

Irani, M., Ismail, H., Ahmad, Z., Fan, M., 2015. Synthesis of linear low-density polyethylene-g-poly (acrylic acid)-co-starch/organo-montmorillonite hydrogel composite as an adsorbent for removal of Pb (II) from aqueous solutions. J. Environ Sci. 27, 9–20.

Jadoun, S., Arif, R., Jangid, N.K., Meena, R.K., 2021. Green synthesis of nanoparticles using plant extracts: A review. Environ. Chem. Lett. 19, 355–374.

Jamshaid, A., Hamid, A., Muhammad, N., Naseer, A., Ghauri, M., Iqbal, J., Rafiq, S., Shah, N.S., 2017. Cellulose-based materials for the removal of heavy metals from wastewater– An overview. ChemBioEng Rev. 4, 1–18.

Javid, N., Malakootian, M., 2017. Removal of bisphenol A from aqueous solutions by modified-carbonized date pits by ZnO nanoparticles. Desalin. Water Treat. 95, 144–151.

Jiang, M., Wang, Q., Jin, X., Chen, Z., 2009. Removal of Pb(II) from aqueous solution using modified and unmodified kaolinite clay. J. Hazard. Mater. 170, 332–339.

Jiang, C., Wang, X., Wang, G., Hao, C., Li, X., Li, T., 2019. Adsorption performance of a polysaccharide composite hydrogel based on crosslinked glucan/chitosan for heavy metal ions. Compos. Part B Eng. 169, 45–54.

Khan, H., Ahmed, M.J., Bhanger, M.I., 2007. A rapid spectrophotometric method for the determination of trace level lead using 1,5-diphenylthiocarbazone in aqueous micellar solutions. Anal. Sci. 2007 (23), 193–199.

Khan, T.A., Dahiya, S., Khan, E.A., 2017. Removal of direct red 81 from aqueous solution by adsorption onto magnesium oxide-coated kaolinite: Isotherm, dynamics and thermodynamic studies. Environ. Prog. Sustain. Energy 36, 45–58.

Khan, M.N., Bashir, O., Khan, T.A., Al-thabaiti, S.A., Khan, Z., 2018. CTAB capped synthesis of bio-conjugated silver nanoparticles and their enhanced catalytic activities. J. Mol. Liq. 258, 133–141.

Khan, S.A., Siddiqui, M.F., Khan, T.A., 2020. Ultrasonic-assisted synthesis of polyacrylamide/bentonite hydrogel nanocomposite for the sequestration of lead and cadmium from aqueous phase: Equilibrium, kinetics and thermodynamic studies. Ultrason. Sonochem. 60, 104761.

Khan, S.A., Hussain, D., Khan, T.A., 2021. Mechanistic evaluation of metformin drug confiscation from liquid phase on itaconic acid/kaolin hydrogel nanocomposite. Environ. Sci. Pollut. Res. 28, 53298–53313.

Khan, S., Idrees, M., Bilal, M., 2021. Revealing and elucidating chemical speciation mechanisms for lead and nickel adsorption on zeolite in aqueous solutions. Colloids Surf. A Physicochem. Eng. 623, 126711.

Khan, S.A., Khan, T.A., 2021. Clay-hydrogel nanocomposites for adsorptive amputation of contaminants from aqueous phase: A review. J. Environ Chem. Eng. 105575.

Khan, T.A., Singh, V., Ali, I., 2009. Sorption of Cd(II), Pb(II), and Cr (VI) metal ions from wastewater using bottom fly ash as a low cost sorbent. J. Environ. Prot. Sci. 3, 124–132.

Khan, T.A., Nazir, M., Khan, E.A., 2016. Magnetically modified multiwalled carbon nanotubes for the adsorption of bismarck brown R and Cd(II) from aqueous solution: batch and column studies. Desalin. Water Treat. 57, 19374–19390.

Khan, T.A., Khan, E.A., Shahjahan., 2015. Removal of basic dyes from aqueous solution by adsorption onto binary iron-manganese oxide coated kaolinite: non-linear isotherm and kinetics modeling. Appl. Clay Sci. 107, 70–77.

Khan, T.A., Mukhlif, A.A., Khan, E.A., Sharma, D.K., 2016. Isotherm and kinetics modeling of Pb(II) and Cd(II) adsorptive uptake from aqueous solution by chemically modified green algal biomass. Model. Earth Syst. 2, 1–13.

Khan, T.A., Nouman, M., Dua, D., Khan, S.A., Alharthi, S.S., 2022. Adsorptive scavenging of cationic dyes from aquatic phase by H_3PO_4 activated Indian jujube (*Ziziphus mauritiana*) seeds based activated carbon: Isotherm, kinetics, and thermodynamic study. J. Saudi Chem. Soc. 26, 101417.

Khatri, Z., Wei, K., Kim, B.-S., Kim, I.-S., 2012. Effect of deacetylation on wicking behavior of co-electrospun cellulose acetate/polyvinyl alcohol nanofibers blend. Carbohydr. Polym. 87, 2183–2188.

Kumar, A.S.K., Kalidhasan, S., Rajesh, V., Rajesh, N., 2012. Application of cellulose-clay composite biosorbent toward the effective adsorption and removal of chromium from industrial wastewater. Ind. Eng. Chem. Res. 51, 58–69.

Lagergren, S., 1898. About the theory of so-called adsorption of soluble substances. K. Sven. 420 Vetenskapsakad. Handl. 24, 1–39.

Langmuir, I., 1918. The adsorption of gases on plane surfaces of glass, mica and platinum. J. Am. Chem. Soc. 40, 1361–1403.

Li, S., Wen, N., Wei, D., Zhang, Y., 2021. Highly effective removal of lead and cadmium ions from wastewater by bifunctional magnetic mesoporous silica. Sep. Purif. Technol. 265, 118341.

Liu, C., Jin, R.-N., Ouyang, X., Wang, Y.-G., 2017. Adsorption behavior of carboxylated cellulose nanocrystal-polyethyleneimine composite for removal of Cr(VI) ions. Appl. Surf. Sci. 408, 77–87.

Malakootian, M., Kannan, K., Gharaghani, M.A., Dehdarirad, A., Nasiri, A., Shahamat, Y.D., Mahdizadeh, H., 2019. Removal of metronidazole from wastewater by Fe/charcoal micro electrolysis fluidized bed reactor. J. Environ. Chem. Eng. 7, 103457.

Manigandana, R., Giribabu, K., Suresh, R., Vijayalakshmi, L., Stephen, A., Narayanan, V., 2013. Cobalt oxide nanoparticles: Characterization and its electrocatalytic activity towards nitrobenzene. Chem. Sci. Trans. 2, S47–S50.

Mnasri-Ghnimi, S., Frini-Srasra, N., 2019. Removal of heavy metals from aqueous solutions by adsorption using single and mixed pillared clays. Appl. Clay Sci. 179, 105151.

Nguyen, D.C.T., Cho, K.Y., Oh, W.-C., 2017. Synthesis of mesoporous SiO_2/Cu_2O–graphene nanocomposites and their highly efficient photocatalytic performance for dye pollutants. RSC Adv. 7, 29284–29294.

Pal, P., Syed, S.S., Banat, F., 2017. Gelatin-bentonite composite as reusable adsorbent for the removal of lead from aqueous solutions: Kinetic and equilibrium studies. J. Water Process Eng. 20, 40–50.

Pawar, R.R., Lalhmunsiama, Kim, M., Kim, J.-G., Hong, S.-M., Sawant, S.Y., Lee, S.M., 2018. Efficient removal of hazardous lead, cadmium, and arsenic from aqueous environment by iron oxide modified clay-activated carbon composite beads. Appl. Clay Sci., 162, 339–350.

Pelalak, R., Heidari, Z., Khatami, S.M., Kurniawan, T.A., Marjani, A., Shirazian, S., 2021. Oak wood ash/GO/Fe_3O_4 adsorption efficiencies for cadmium and lead removal from aqueous solution: Kinetics, equilibrium and thermodynamic evaluation. Arab. J. Chem. 14, 102991.

Qin, L., Yan, L., Chen, J., Liu, T., Yu, H., Du, B., 2016. Enhanced Removal of Pb^{2+}, Cu^{2+}, and Cd^{2+} by amino-functionalized magnetite/kaolin clay. Ind. Eng. Chem. Res. 55, 7344–7354.

Sahraei, R., Ghaemy, M., 2017. Synthesis of modified gum tragacanth/graphene oxide composite hydrogel for heavy metal ions removal and preparation of silver nanocomposite for antibacterial activity. Carbohydr. Polym. 157, 823–833.

Saravaia, H., Gupta, H., Popat, P., Sodha, P., Kulshrestha, V., 2018. Single-Step Synthesis of Magnesium-Doped Lithium Manganese Oxide Nanosorbent and Their Polymer Composite Beads for Selective Heavy Metal Removal. ACS Appl. Mater. Interfaces 10, 44059–44070.

Sari, A., Tuzen, M., 2014. Cd(II) adsorption from aqueous solution by raw and modified kaolinite. Appl. Clay Sci. 88-89, 63–72.

Sellaoui, L., Soetaredjo, F.E., Ismadji, S., Bonilla-Petriciolet, A., Belver, C., Bedia, J., Ben Lamine, A., Erto, A., 2018. Insights on the statistical physics modeling of the adsorption of Cd^{2+} and Pb^{2+} ions on bentonite-chitosan composite in single and binary systems. Chem. Eng. J. 354, 569–576.

Shamsudin, M.S., Azha, S.F., Shahadat, M., Ismail, S., 2019. Cellulose/bentonite-zeolite composite adsorbent material coating for treatment of N-based antiseptic cationic dye from water. J. Water Process Eng. 29, 100764.

Singh, S., Basu, H., Bassan, M.K.T., Singhal, R.K., 2022. Thiol functionalised silica microsphere loaded polymeric hydrogel: Development of a novel hybrid sorbent for removal of lead and cadmium. Chemosphere 286, 131659.

Soltani, R., Dinari, M., Mohammadnezhad, G., 2018. Ultrasonic-assisted synthesis of novel nanocomposite of poly(vinyl alcohol) and amino-modified MCM-41: A green adsorbent for Cd(II) removal. Ultrason. Sonochem. 40, 533–542.

Tabesh, S., Davar, F., Loghman-Estarki, M.R., 2018. Preparation of γ-Al_2O_3 nanoparticles using modified sol-gel method and its use for the adsorption of lead and cadmium ions. J. Alloys Compd. 730, 441–449.

Temkin, M.I., 1940. Kinetics of ammonia synthesis on promoted iron catalysts. Acta Physiochim. URSS 12, 327–356.

Venkateswarlu, S., Kumar, B.N., Prathima, B., SubbaRao, Y., Jyothi, N.V.V., 2019. A novel green synthesis of Fe_3O_4 magnetic nanorods using *Punica granatum* rind extract and its application for removal of Pb(II) from aqueous environment. Arab. J. Chem. 12, 588–596.

Vidovix, T.B., Quesada, H.B., Januário, E.F.D., Bergamasco, R., Vieira, A.M.S., 2019. Green synthesis of copper oxide nanoparticles using *Punica granatum* leaf extract applied to the removal of methylene blue. Mater. Lett. 257, 126685.

Wan Ngah, W.S., Teong, L.C., Hanafiah, M.A.K.M., 2011. Adsorption of dyes and heavy metal ions by chitosan composites: A review. Carbohydr. Polym. 83, 1446–1456.

Wang, N., Ouyang, X.-K., Yang, L.-Y., Omer, A.M., 2017. Fabrication of a magnetic cellulose nanocrystal/metal–organic framework composite for removal of Pb(II) from water. ACS Sustain. Chem. Eng. 5, 10447–10458.

Ab Latif Wani, A.A., Usmani, J.A., 2015. Lead toxicity: a review. Interdiscip. Toxicol., 8(2), 55.

Weber, W.J., Morris, J.C., 1963. Kinetics of adsorption on carbon from solution. J. Sanit. Eng. Div. Am. Soc. Civ. Eng. 89, 31–60.

Yadav, V.B., Gadi, R., Kalra, S., 2019. Clay based nanocomposites for removal of heavy metals from water: A review. J. Environ. Manag. 232, 803–817.

Yan, J., White, K., Yu, D.-G., Zhao, X.-Y., 2014. Sustained-release multiple-component cellulose acetate nanofibers fabricated using a modified coaxial electrospinning process. J. Mater. Sci. 49, 538–547.